The Company of
Biologists

RESEARCH ARTICLE

Timely Schwann cell division drives peripheral myelination *in vivo* via the laminin/cAMP pathway

Aya Mikdache*,‡, Marie-José Boueid‡, Emilie Lesport, Brigitte Delespierre, Julien Loisel-Duwattez, Cindy Degerny§ and Marcel Tawk§

ABSTRACT

Schwann cells (SCs) migrate along peripheral axons and divide intensively to generate the right number of cells prior to axonal ensheathment; however, little is known regarding the temporal and molecular control of their division and its impact on myelination. We report that Sil, a spindle pole protein associated with autosomal recessive primary microcephaly, is required for temporal mitotic exit of SCs. In *sil*-deficient *cassiopeia* ($csp^{-/-}$) mutants, SCs fail to radially sort and myelinate peripheral axons. Elevation of cAMP, but not Rac1 activity, in $csp^{-/-}$ restores myelin ensheathment. Most importantly, we show a significant decrease in laminin expression within $csp^{-/-}$ posterior lateral line nerve and that forcing Laminin 2 expression in $csp^{-/-}$ fully restores the ability of SCs to myelinate. Thus, we demonstrate an essential role for timely SC division in mediating laminin expression to orchestrate radial sorting and peripheral myelination *in vivo*.

KEY WORDS: *Sil*, Schwann cell, Peripheral nervous system, Mitotic spindle, MCPH, Zebrafish, Myelin, PLLn, Mitosis, Laminin, cAMP

INTRODUCTION

Schwann cells (SCs) are the myelinating glia that ensure efficient nerve impulse conduction along the nerves of the peripheral nervous system (Jessen and Mirsky, 2005; Woodhoo and Sommer, 2008; Herbert and Monk, 2017; Bouçanova and Chrast, 2020; Raphael et al., 2011; Pereira et al., 2012; Sherman and Brophy, 2005). In order to myelinate, SCs go through a series of developmental changes that include (1) migration and division along peripheral axons, (2) intensive proliferation prior to axonal ensheathment such that one SC myelinates one axonal segment and (3) substantial cytoskeletal rearrangements and changes in cell shape that allow a SC to radially sort an axon in a 1:1 ratio, a process termed radial sorting (Monk et al., 2015; Raphael and Talbot, 2011; Feltri et al., 2016). The latter enables SCs to extend their processes along a unique abaxonal-adaxonal polarity axis in order to select and sort an axon to myelinate (Tricaud, 2018). It has been shown *in vitro* that SCs first secrete and assemble their own basal lamina (Eldridge et al., 1989; Colognato and Tzvetanova, 2011) that would later on regulate, through receptor interactions, different signals required for SC proliferation, survival and differentiation (Chen and Strickland,

2003; Nodari et al., 2008, 2007; Court et al., 2009; Yu et al., 2005; Yamada et al., 1996). Of particular interest are the extracellular matrix (ECM) proteins laminins and collagens that play essential roles in SC development (Chernousov et al., 2008).

However, several issues regarding the characteristics of timely SC division during migration and radial sorting, as well as the coupling of division with ECM proteins and myelination *in vivo*, remain unresolved.

The mitotic spindle is a bipolar array of microtubules that mediates chromosome separation during cell division (Hara and Fukagawa, 2020; Petry, 2016). The organization and temporal assembly of the spindle are all important features that dictate the outcome of division (Lu and Johnston, 2013). One crucial aspect of cell division is the temporal control of mitosis; this is highlighted by the existence of a mitotic spindle checkpoint that ensures accurate mitotic spindle organization prior to anaphase (Lara-Gonzalez et al., 2012). A great number of proteins is involved in spindle organization; one such major player is Sil (also known as Stil), which is ubiquitously expressed and specifically localizes to the poles of the mitotic spindle in metaphase cells (Pfaff et al., 2007; Campaner et al., 2005). The *sil* gene was originally cloned from leukemia-associated chromosomal translocation and is overexpressed in several tumor types (Aplan et al., 1991, 1990). It is associated with autosomal recessive primary microcephaly (MCPH), a neurogenic mitotic disorder that results in significantly reduced brain size (Naveed et al., 2018; Zaqout et al., 2017). Studies of the zebrafish *cassiopeia* mutant ($csp^{-/-}$), which has a nonsense mutation in, and therefore loss of function of *sil*, show abnormalities in prometaphase progression within retinal neuroepithelium (Novorol et al., 2013). Thus, *sil* represents an ideal candidate to study for a role in mitotic synchronization and division during SC development.

Here, we used live imaging, genetics and pharmacological tools in zebrafish to monitor SC behavior during its division and unraveled for the first time an essential role for timely Schwann cell division in peripheral myelination. We identified Sil as a crucial regulator of SC radial sorting and myelination. Time-lapse imaging revealed an important role for *sil* in SC metaphase progression; loss of Sil resulted in delayed mitotic exit and caused a complete loss of axonal ensheathment as revealed by transmission electron microscopy (TEM). Treating $csp^{-/-}$ with forskolin, which binds to adenyl cyclase and elevates the levels of cAMP, or forcing Laminin 2 expression was sufficient to fully restore peripheral myelination.

RESULTS
SCs show a regular pattern of division along the posterior lateral line nerve

In order to monitor SC division, we took advantage of the *Tg(foxd3: gfp)* line (Gilmour et al., 2002) and imaged SCs along the posterior lateral line nerve (PLLn) during early migration, i.e. between 24 and

DEVELOPMENT

42 h post-fertilization (hpf) and during radial sorting (between 48 and 60 hpf) (Fig. 1A) (Lyons et al., 2005; Raphael et al., 2011). SCs were generally elongated during migration until they went through mitotic rounding, divided and then re-elongated (Fig. 1B, Movie 1). SCs divided along the anterior-posterior (AP) axis of the embryo and it took an average of 9.81±0.63 min (mean±s.e.m.) for them to complete cytokinesis. To assess the importance of this pattern of division in SC myelination, we monitored their behavior in the zebrafish *cassiopeia* mutant ($csp^{-/-}$). Sil is a ubiquitously expressed protein that specifically localizes to the mitotic spindle in metaphase cells and plays a crucial role in its organization (Pfaff et al., 2007; Novorol et al., 2013). SCs struggled to exit mitosis in $csp^{-/-}$ with an average of 87.20±4.72 min for cytokinesis to be completed (Fig. 1B,C, Movie 2). However, re-elongation of SCs occurred normally after division in both mutants and controls (Fig. 1B). The

same result was obtained during radial sorting; SCs became elongated along the axons until they went through mitotic rounding, leading to division, and then re-elongated again (Fig. 1D). Cells divided along the AP axis of the embryo and it took an average of 9.30±0.61 min for cytokinesis to complete (Fig. 1E, Movie 3). SC cytokinesis in $csp^{-/-}$ took much longer to complete with an average of 90.10±14.13 min (Fig. 1D,E, Movie 4).

This result suggests that Sil deficiency leads to a significant delay in SC cytokinesis.

SCs in $csp^{-/-}$ show delays in mitotic progression but exit mitosis with no significant increase in apoptosis

sil is ubiquitously expressed but highly enriched in neural cells and $csp^{-/-}$ embryos show major neuronal defects, such as an increase in the percentage of mitotically arrested neuroepithelial cells in the
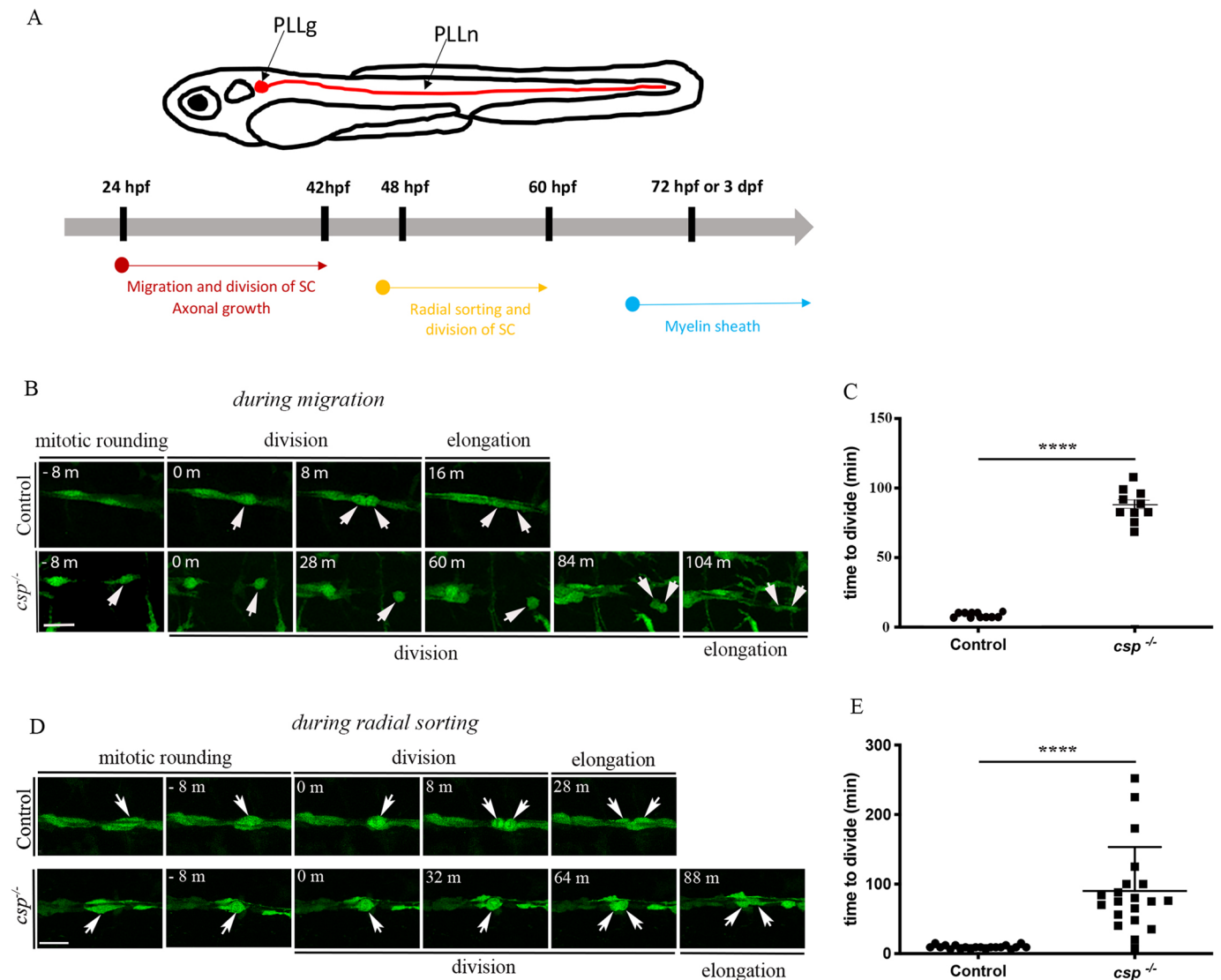

Fig. 1. SCs show a regular pattern of division during migration and radial sorting. (A) Timeline of SC behavior and myelination in zebrafish. SCs migrate and divide along growing axons between 24 hpf and 48 hpf. They start to radially sort axons of the PLLn at around 48 hpf and divide intensively. The myelin sheath was analyzed starting from 3 dpf (or 72 hpf). (B) Still images of time-lapse imaging in *Tg(foxd3:gfp)* control and *Tg(foxd3:gfp)/csp*$^{-/-}$ embryos at around 30 hpf. Arrows indicate SCs along the PLLn at different time points prior to and after division. Scale bar: 20 µm. (C) Quantification of the time required for control (11 cells from three different embryos) and $csp^{-/-}$ (ten cells from three different embryos) SCs to successfully complete cytokinesis during migration (****$P \le 0.0001$). (D) Still images of time-lapse imaging in *Tg(foxd3:gfp)* control and *Tg(foxd3:gfp)/csp*$^{-/-}$ embryos at around 52 hpf. Arrows indicate SCs along the PLLn at different time points prior to and after division. Scale bar: 20 µm. (E) Quantification of the time required for control (20 cells from six different embryos) and $csp^{-/-}$ (20 cells from five different embryos) SCs to successfully complete cytokinesis (****$P \le 0.0001$). m, minutes.

retina that coincides with an increase in apoptosis (Novorol et al., 2013). To test whether this is the case for SCs, we first labeled SCs using the M-phase marker PH3 in the *Tg(foxd3:gfp)* line. As seen in the retina (Novorol et al., 2013), we observed a significant increase in the fraction of proliferating PH3$^+$ SCs at 48 hpf. This coincided with a decrease in the total number of SCs and an increase in the percentage of PH3$^+$ SCs relative to the total number of SCs counted within a defined region (Fig. 2). However, the number of PH3$^+$ SCs and the percentage of PH3$^+$ SCs relative to the total number of SCs were normal at 72 hpf (Fig. 2). The total number of SCs remained significantly lower in $csp^{-/-}$ at 72 hpf in comparison with controls (Fig. 2B). Time-lapse analysis using the nuclear marker *h2b:gfp* pointed to a delay in prometaphase progression (Fig. S1A, Movies 5 and 6). However, in contrast to the neuronal phenotype in retina and spinal cord, most SCs exited mitosis and we detected no increase in apoptotic SCs in these mutants along the PLLn (Fig. S1B-D).

These data suggest that *sil* is required for the temporal control of mitotic exit of SCs; nevertheless, SCs devoid of *sil* do exit mitosis following a significant delay and are not apoptotic.

Sil is essential for SC radial sorting and myelination

Having identified a delay in progression through mitosis in SCs and a decrease in the total number of SCs in $csp^{-/-}$, we wondered whether these defects have any impact on the ability of SCs to ensheath axons. TEM analysis showed a dramatic decrease in the number of myelinated axons in $csp^{-/-}$ in comparison with controls. We observed an average of 5.6±0.55 myelinated axons per nerve in controls in comparison to zero myelinated axons per nerve in $csp^{-/-}$ at 72 hpf [or 3 days post-fertilization (dpf)] (Fig. 3A-A″,B,E). In addition, we observed a significant decrease in the total number of axons in these mutants with an average of 55±2.85 axons in controls and 28.63±2.67 in $csp^{-/-}$ PLLn (Fig. 3F). The myelination defect in $csp^{-/-}$ embryos was also observed at 4 dpf (Fig. 3C-F). This analysis could not be extended to later stages because $csp^{-/-}$ embryos died at 5 dpf.

Given the drastic decrease in total number of axons in these mutants, we calculated the ratio of myelinated axons relative to the total number of axons in the PLLn. Whereas we counted an average of 10.46±1.14% of myelinated axons in controls at 3 dpf and 15.44±0.87% at 4 dpf, we observed 0% in $csp^{-/-}$ at 3 and 4 dpf (Fig. 3G). This myelination defect was not the result of a decrease in
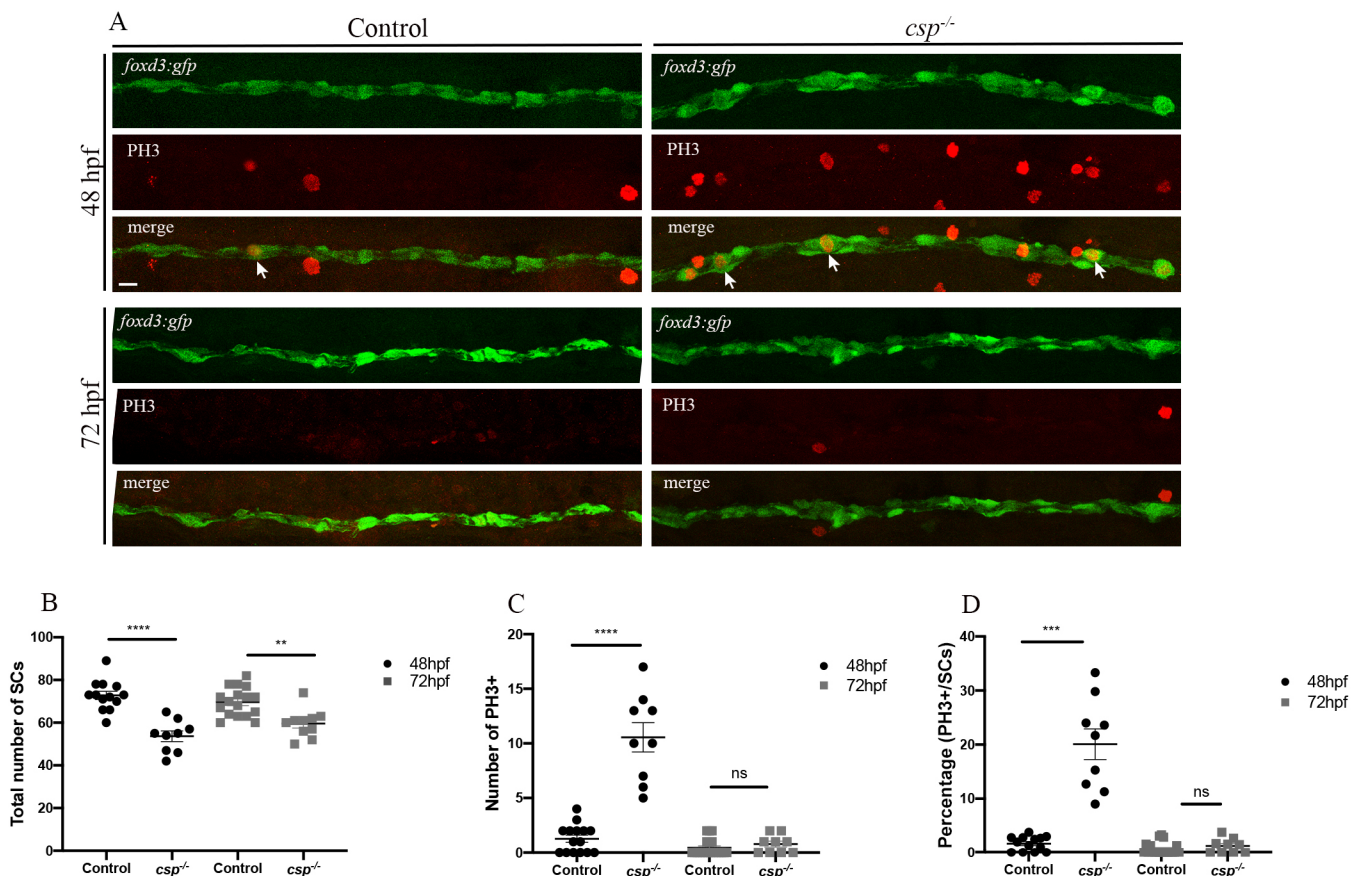

Fig. 2. SCs in $csp^{-/-}$ show delays in mitotic progression but exit mitosis with no significant increase in apoptosis. (A) PH3 immunolabeling in *Tg(foxd3:gfp)* and *Tg(foxd3:gfp)/csp$^{-/-}$* larvae at 48 hpf and 72 hpf. Arrows indicate SCs that are GFP and PH3 positive. Scale bar: 25 µm. (B) Quantification of the number of SCs within a defined region of the PLLn at 48 and 72 hpf in control (average of 72.77±1.96 cells at 48 hpf, *n*=13 embryos; average of 69.60±1.61 cells at 72 hpf, *n*=17 embryos) and $csp^{-/-}$ (average of 53.67±2.50 cells at 48 hpf, *n*=9 embryos; average of 59.60±2.10 cells at 72 hpf, *n*=10 embryos) (****P≤0.0001; **P=0.0012). (C) Quantification of the number of PH3$^+$ SCs within a defined region of the PLLn at 48 and 72 hpf in control (average of 1.26±0.33 cells at 48 hpf, *n*=15 embryos; average of 0.45±0.17 cells at 72 hpf, *n*=20 embryos) and $csp^{-/-}$ (average of 10.56±1.34 cells at 48 hpf, *n*=9 embryos; average of 0.77±0.27 cells at 72 hpf, *n*=9 embryos) (****P≤0.0001; ns, P=0.33). (D) Quantification of the percentage of PH3$^+$ SCs relative to the total number of SCs within a defined region of the PLLn at 48 and 72 hpf in control (average of 1.68±0.38 cells at 48 hpf, *n*=13 embryos; average of 0.67±0.26 cells at 72 hpf, *n*=20 embryos) and $csp^{-/-}$ (average of 20.08±2.83 cells at 48 hpf, *n*=9 embryos; average of 1.25±0.46 cells at 72 hpf; *n*=9 embryos) (***P=0.0002; ns, P=0.19).
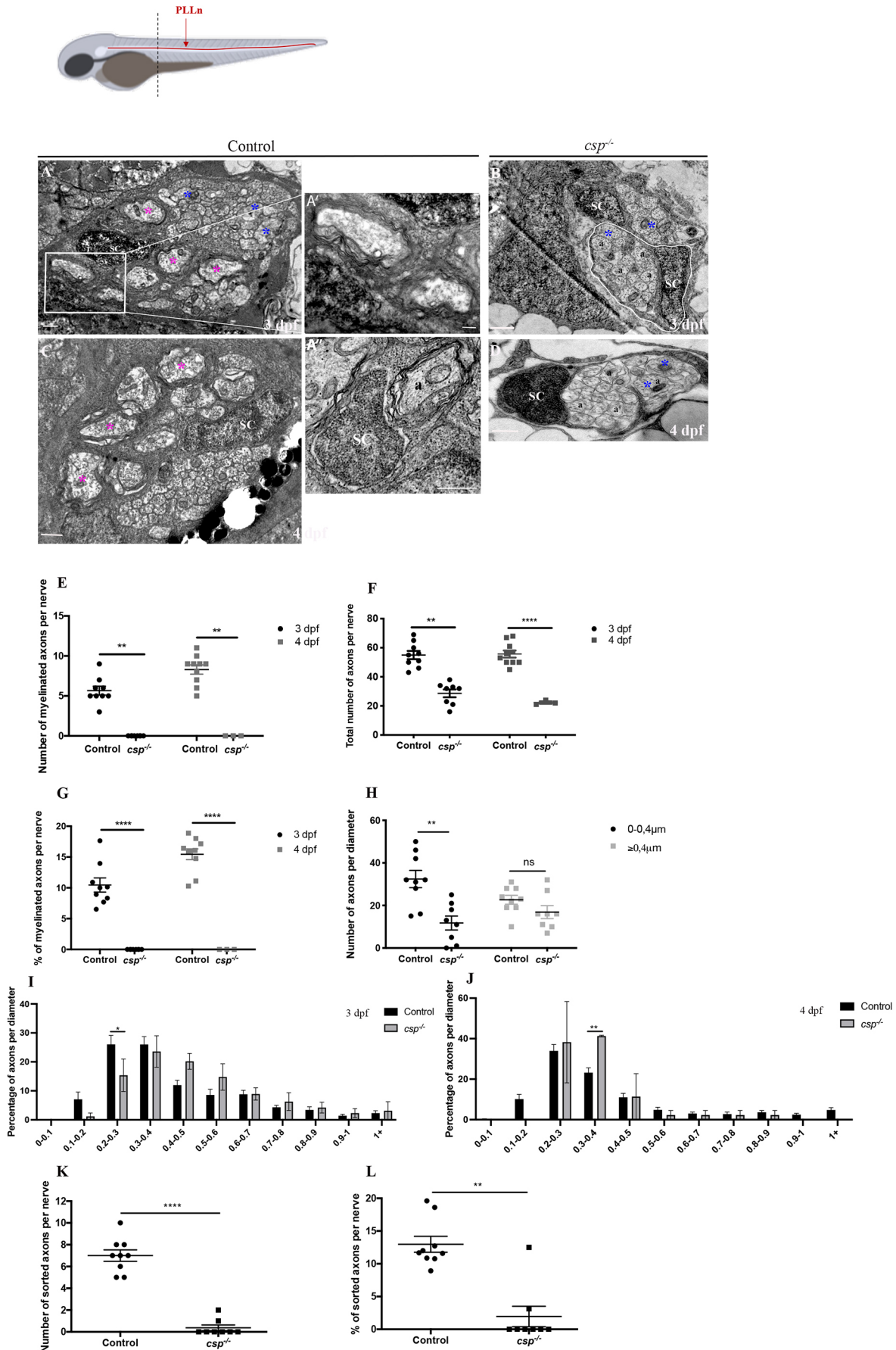
Fig. 3. See next page for legend.

Fig. 3. Sil is essential for radial sorting and myelination by SCs.
Schematic at the top shows a zebrafish larvae with PLLn shown in red. The dotted line represents the AP position of the cross-section analysis by TEM. (A-D) TEM of a cross-section of the PLLn at 3 dpf in control (A,A′) and $csp^{-/-}$ (B) and at 4 dpf in control (C) and $csp^{-/-}$ (D). Magenta asterisks highlight some large caliber myelinated axons (also shown at higher magnification in A′) and blue asterisks show some large caliber non-myelinated axons. Scale bars: 0.5 μm (A,A″,B-D); 0.2 μm (A′). (A″) Example of a 1:1 association between a SC and an axon at 3 dpf (from a different control embryo). a, axon. Axons remained bundled in $csp^{-/-}$ such that one SC was associated with a bundle of axons, delineated in white in B. (E) Quantification of the number of myelinated axons per nerve at 3 dpf in controls (nine nerves, n=5 embryos) and $csp^{-/-}$ (eight nerves, n=6 embryos) and at 4 dpf in controls (average of 8.3±0.57 myelinated axons; ten nerves, n=6 embryos) and $csp^{-/-}$ (zero myelinated axons; three nerves, n=3 embryos) (**P=0.0035 at 3 dpf; **P=0.005 at 4 dpf). (F) Quantification of the total number of axons per nerve at 3 dpf in controls and $csp^{-/-}$ and at 4 dpf in controls (54±3.16 axons) and $csp^{-/-}$ (23±1 axons) (**P=0.003; ****P≤0.0001). (G) Quantification of the percentage of myelinated axons relative to the total number of axons per nerve at 3 and 4 dpf in controls and $csp^{-/-}$ (****P≤0.0001). (H) Quantification of the number of axons relative to their diameter at 3 dpf in controls (average of 32.44 for 0-0.4 μm; average of 22.67 for >0.4 μm) and $csp^{-/-}$ (average of 11.75 for 0-0.4 μm; average of 16.88 for >0.4 μm) (**P=0.0013; ns, P=0.14). (I) Graph representing the distribution of axons relative to their diameter with 0.1 μm bin width at 3 dpf in controls and $csp^{-/-}$ embryos (*P=0.04). (J) Graph representing the distribution of axons relative to their diameter with 0.1 μm bin width at 4 dpf in controls and $csp^{-/-}$ embryos (**P=0.0015). (K) Quantification of the number of sorted axons per nerve at 3 dpf in control (average of 7.00±0.52) and $csp^{-/-}$ (0.37±0.26) embryos (****P≤0.0001). (L) Quantification of the percentage of sorted axons relative to the total number of axons at 3 dpf in control (12.97±1.21) and $csp^{-/-}$ (1.95±1.55) embryos (**P=0.0019).

the number of large caliber axons (diameter ≥0.4 μm) that should be myelinated (Fig. 3H). We also analyzed the distribution of axons relative to their diameter with a 0.1 μm bin width at 3 dpf and only the percentage of a group of small caliber axons (0.2-0.3 μm) was slightly but significantly decreased in $csp^{-/-}$ (Fig. 3I). We even observed a significant increase in the percentage of axons with 0.3-0.4 μm diameter in $csp^{-/-}$ at 4 dpf in comparison with controls (Fig. 3J). Finally, the myelination defect coincided with a significant decrease in the number and the percentage of radially sorted axons per nerve (Fig. 3K,L).

These results show that *sil* is required for SC radial sorting and myelination.

Sil is required within SCs for axonal wrapping and normal Mbp expression and regulates the number of neurons within the posterior lateral line ganglia

To test whether the myelination defect observed here is specific to SCs or secondary to neuronal defects, we first examined several aspects of posterior lateral line ganglia (PLLg) and PLLn development. $csp^{-/-}$ embryos presented no major defects in PLLn growth and SC migration at 48 hpf (Fig. S2A). A few $csp^{-/-}$ embryos (<30%, n=7/24) showed an axonal growth arrest but posterior to the yolk extension and SCs were found at the tip end of these axons. We next analyzed axonal transport along the PLLn using a *mito:gfp* construct, which labels mitochondria. We observed no significant difference in the speed of mitochondrial movement along the PLLn with an average of 1.92±0.14 μm/s and 1.85±0.06 μm/s in controls and $csp^{-/-}$, respectively (Fig. S2B,C, Movies 7 and 8). We next counted the number of neurons within the PLLg and observed a significant decrease in $csp^{-/-}$ embryos (Fig. S2D,E) that coincided with the reduction in the number of axons in the PLLn.

These results suggest a role for *sil* in the development of PLLg, but not in axonal growth or transport.

To test directly whether *sil* has an autonomous function in SC myelination, we forced the expression of *sil* specifically in SCs under the control of the *sox10* promoter. $csp^{-/-}$ embryos were injected with *pTol2-sox10:sil-P2A-mCherry-CaaX* and *tol2* transposase mRNA at the one-cell stage and selected at 3 dpf for continuous mCherry expression in SCs at the level of yolk extension. By forcing the expression of *sil* specifically in SCs, we significantly increased the number of myelinated axons in $csp^{-/-}$ embryos at 3 dpf (Fig. 4A-C″). The percentage of myelinated axons per nerve in injected $csp^{-/-}$ embryos was similar to that observed in controls (Fig. 4D). We observed no significant difference in the distribution of axons relative to their diameter with 0.1 μm bin width at 3 dpf between the three groups (Fig. 4E).

We also processed control and $csp^{-/-}$ larvae for immunohistochemistry to detect Mbp at 3 dpf. We observed a significant decrease in Mbp expression in $csp^{-/-}$ embryos (Fig. 4F-G″). We then injected $csp^{-/-}$ embryos with *pTol2-sox10:sil-P2A-mCherry-CaaX* and *tol2* transposase mRNA at the one-cell stage and selected embryos for mosaic mCherry$^+$ clonal analysis. We analyzed four mutant larvae that had *sox10*:mCherry$^+$ SCs along mutant PLLn; the mCherry$^+$ clones appeared to express normal levels of Mbp (Fig. 4H-I″).

Altogether, these results suggest a specific requirement for *sil* within SCs to initiate axonal wrapping and Mbp expression.

Forcing cAMP activity, via forskolin treatment, rescues radial sorting, myelin gene expression and axonal wrapping defects in $csp^{-/-}$

M phase is characterized by chromatin condensation and temporal ejection of transcription factors (Ma et al., 2015). Given that *sil* is implicated in spindle checkpoint and mitotic progression during M phase, it is possible that the delayed mitotic exit observed in $csp^{-/-}$ embryos could result in prolonged ejection of transcription factors required for myelination in SCs. Alternatively, it is possible that transcriptional activity is effective after mitosis, but SCs in $csp^{-/-}$ embryos present defective upstream signaling activity. To distinguish between these possibilities, we first analyzed the expression of *krox20* (*egr2b*) and *mbp* (*mbpa*) in controls and $csp^{-/-}$ embryos at 52 hpf and 3 dpf, respectively. $csp^{-/-}$ embryos showed a sharp decrease in the expression of peripheral myelin genes (Fig. 5A,B,D,E). This coincided, as shown before, with a total lack of radial sorting and axonal ensheathment (Fig. 5H). Second, we decided to treat embryos with forskolin (FSK), which interacts with adenyl cyclase and elevates the levels of cAMP. When $csp^{-/-}$ embryos were treated with FSK during radial sorting, the expression of *krox20* and *mbp* was restored (Fig. 5C,F), as well as the ratio of myelinated axons relative to the total number of axons (Fig. 5I,J). The distribution of axons relative to their diameter with 0.1 μm bin width at 3 dpf between the two groups of $csp^{-/-}$ and $csp^{-/-}$+FSK embryos was not altered, even though some significant differences were observed between controls and $csp^{-/-}$+FSK embryos (Fig. 5K). We also labeled SCs with the M-phase marker PH3 and observed a significant decrease in the total number of SCs between FSK-treated and non-treated (control) groups (Fig. 5L), but the decrease was not significant between $csp^{-/-}$ and $csp^{-/-}$+FSK embryos. However, the number of PH3$^+$ SCs and the percentage of PH3$^+$ SCs were significantly decreased in $csp^{-/-}$+FSK in comparison with $csp^{-/-}$ embryos (Fig. 5M,N). We also used time-lapse imaging to track SC division in $csp^{-/-}$+FSK embryos and we could only detect two dividing cells from six different embryos (36 h recording in total) because proliferation was almost blocked in these embryos. However, dividing SCs took as long as 121 min to complete
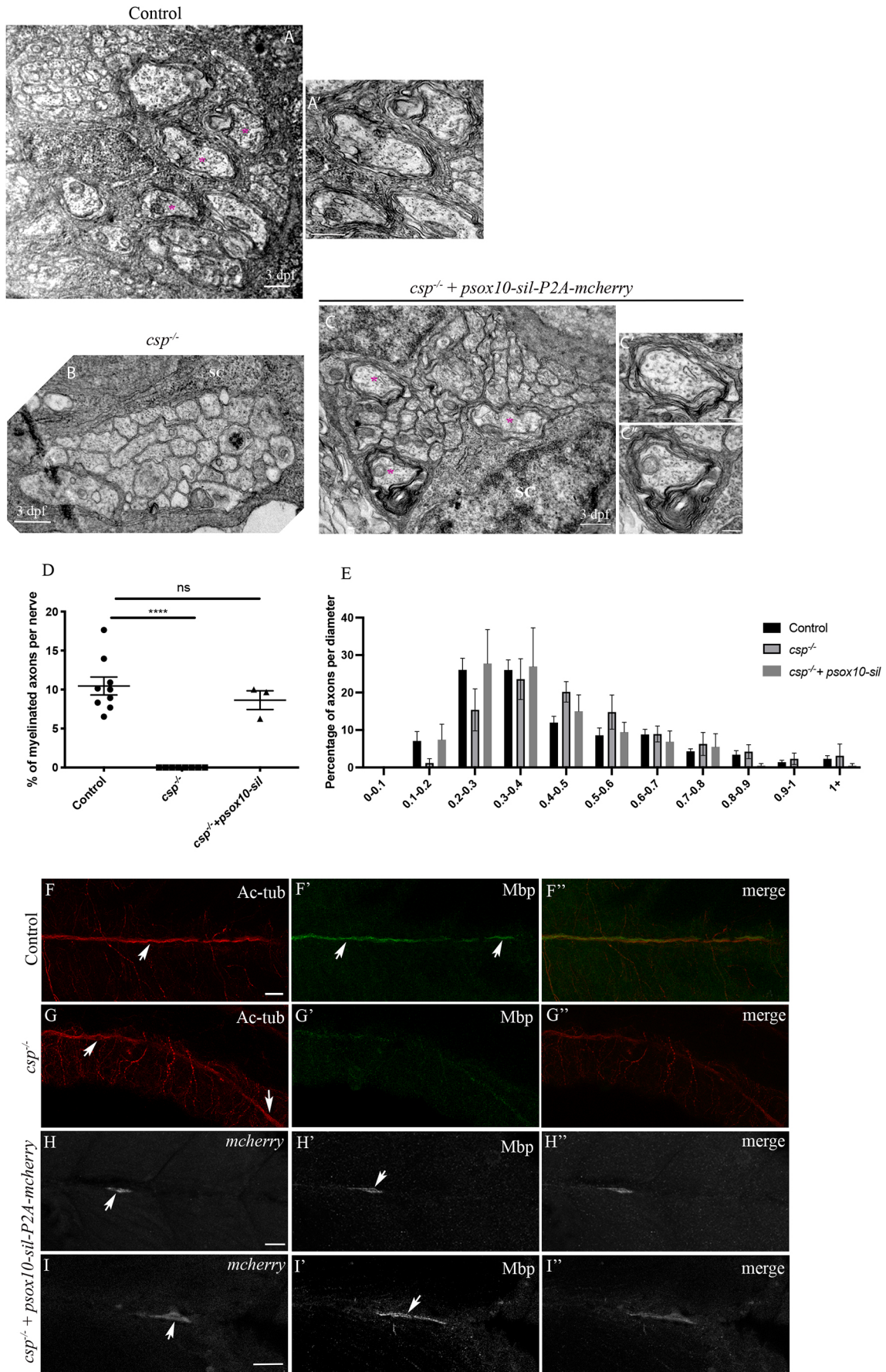
Fig. 4. See next page for legend.

Fig. 4. Sil is required within SCs for axonal wrapping. (A-C″) TEM of a cross-section of the PLLn at 3 dpf in control (A,A′), $csp^{-/-}$ (B) and $csp^{-/-}$ embryos injected with *psox10-sil-P2A-mCherry* (C-C″). Magenta asterisks indicate some large caliber myelinated axons (shown at higher magnification in A′, C′, C″). Scale bars: 0.5 μm (A-C); 0.2 μm (C′,C″). (D) Quantification of the percentage of myelinated axons relative to the total number of axons in control (average of 10.46±1.14%, nine nerves, *n*=5 embryos), $csp^{-/-}$ (0%, eight nerves, *n*=6 embryos) and $csp^{-/-}$ injected with *psox10-sil-P2A-mCherry* (average of 8.64±1.20%, three nerves, *n*=3 embryos) (****$P \leq 0.0001$; ns, $P=0.4871$). (E) Graph representing the distribution of axons relative to their diameter with 0.1 μm bin width at 3 dpf in controls, $csp^{-/-}$ and $csp^{-/-}$ embryos injected with *psox10-sil-P2A-mCherry*. (F-I″) Acetylated tubulin (Ac-tub) and Mbp immunolabeling in control (F-F″), $csp^{-/-}$ (G-G″) and $csp^{-/-}$+*psox10-sil-P2A-mCherry* (H-I″) embryos at 3 dpf. Arrows indicate the PLLn in F and G, the myelin sheaths in F′, mCherry⁺ Schwann cells along the PLLn in H and I and the corresponding Mbp expression in H′ and I′. F″, G″, H″ and I″ are the corresponding merge images of F and F′, G and G′, H and H′, I and I′, respectively. Scale bars: 20 μm.

cytokinesis, highlighting a defective progression through mitosis as observed in $csp^{-/-}$.

This result suggests that SCs in $csp^{-/-}$ are still capable of activating the transcriptional program for terminal myelination. It also shows that FSK treatment significantly decreases the number of proliferating SCs in $csp^{-/-}$ while prompting differentiation.

Forcing Rac1 activity does not rescue radial sorting and myelination defects in $csp^{-/-}$

The radial sorting defect and lack of axonal ensheathment by SCs observed in this mutant might also be linked to a defective cytoskeletal re-arrangement. To test this hypothesis, we forced the expression of Rac1, a small GTPase protein that interacts with SC cytoskeleton (Nodari et al., 2007) and is able to restore peripheral radial sorting defects in zebrafish (Mikdache et al., 2020; Boueid et al., 2020). $csp^{-/-}$ embryos injected with a constitutive active form of Rac1 were comparable to non-injected $csp^{-/-}$ embryos and showed a total lack of radial sorting and axonal ensheathment (Fig. S3A,B).

This result suggests that $csp^{-/-}$ myelin defects do not ensue from defective Rac1 activity.

Forcing Laminin α2 expression fully rescues myelination defects in $csp^{-/-}$

Previous studies have shown that Laminin 211 promotes myelination via a GPR126/cAMP-dependent pathway (Petersen et al., 2015); given that FSK treatment of $csp^{-/-}$ embryos is sufficient to re-establish myelination in these mutants, we hypothesized that Laminin 211 expression and/or function might be impaired in these mutants. To test this, we first analyzed laminin expression at 48 hpf in controls and $csp^{-/-}$ embryos by immunostaining. Indeed, laminin expression was significantly reduced along the PLLn of $csp^{-/-}$ embryos (Fig. 6A-C). We next wondered whether increasing extracellular Lama2 levels would rescue the myelination defect. To this end, we took advantage of a *lama2* overexpression construct that expresses membrane EGFP as well as secreted mCherry-tagged Lama2 under the control of muscle-specific *skeletal-alpha actin* (*acta1*) promoter (denoted *pacta1*) (Sztal et al., 2012; Petersen et al., 2015) and injected 20 pg of this construct into $csp^{-/-}$ mutants. Embryos that showed significant expression of EGFP within muscles surrounding the PLLn and mCherry-tagged laminin within the PLLn itself (Fig. 6D,E) were then selected and analyzed by TEM at 3 dpf. Injected $csp^{-/-}$ embryos showed a significant increase in the number of myelinated axons in comparison with non-injected

$csp^{-/-}$ larvae and were comparable to controls (wild-type *lama2*-injected embryos) with respect to the percentage of myelinated axons relative to the total number of axons (Fig. 6F-J). The distribution of axons relative to their diameter with 0.1 μm bin width at 3 dpf between $csp^{-/-}$ and $csp^{-/-}$ injected with *pacta1-lama2* showed a significant increase in groups of small caliber axons (0.1-0.3 μm) but axons of other sizes were not altered (Fig. 6K).

These results strongly suggest defective laminin expression and function within the PLLn of $csp^{-/-}$ mutant, which is responsible for the radial sorting and myelination defect.

Laminin 2 is known to control several aspects of SC development, such as proliferation and differentiation (Chernousov et al., 2008). We therefore wondered whether Lama2 overexpression impacts the timely division and/or proliferation of SCs to mediate myelination or whether the radial sorting/myelination process is triggered by Lama2 regardless of the number of SCs. To investigate this, we used the M-phase marker PH3 and time-lapse imaging to monitor dividing SCs. We observed a significant reduction in the number of SC in control and $csp^{-/-}$ embryos injected with *pacta1-lama2* in comparison with their respective non-injected controls as well as the percentage of PH3⁺ SCs in $csp^{-/-}$ injected with *pacta-lama2* in comparison with non-injected $csp^{-/-}$ (Fig. 7A-C). Time-lapse analysis showed a delay in SC mitotic exit similar to that observed in $csp^{-/-}$ embryos during migration and prior to axonal ensheathment (Fig. 7D,E).

This result strongly suggests that the myelination defect observed in $csp^{-/-}$ is due to a defective laminin pathway and that a reduction in SC numbers is not essential for myelination to proceed.

SCs are a major source of laminin within the PLLn and forcing Laminin α2 expression within SCs rescues Mbp expression in $csp^{-/-}$

It remained important to determine the source of laminin within the PLLn and whether SC-specific expression of laminin would rescue myelination autonomously in *sil* mutants. To investigate this, we first incubated embryos with AG1478, which specifically blocks ErbB signaling in zebrafish and inhibits SC migration along the PLLn (Lyons et al., 2005). Embryos treated with AG1478 between 24 and 48 hpf presented no SCs along the PLLn and showed a significant decrease in laminin expression at 48 hpf (Fig. 8A-C).

Second, we designed a p*UAS-lama2-EGFP-mCherry* construct and took advantage of the *tg(sox10:Gal4VP16)* line to allow a specific expression of Lama2 within SCs (EGFP⁺ labeling); Lama2 is also found secreted within the PLLn (mCherry⁺ labeling) (Fig. 8D-E‴). We injected 20 pg of plasmid in *sox10:Gal4VP16* and $csp^{-/-}$/*sox10:Gal4VP16* embryos at the one-cell stage and proceeded with EGFP and Mbp immunostaining for clonal analysis at 3 dpf. Injected $csp^{-/-}$ embryos that showed expression of EGFP in SCs along the PLLn expressed normal levels of Mbp, whereas those that were negative for EGFP labeling showed a significant decrease in Mbp expression similar to that in non-injected $csp^{-/-}$ larvae (Fig. 8F-H″).

These results strongly suggest that timely SC division is largely responsible for laminin expression within the PLLn. This constitutes a crucial step for timely myelination.

DISCUSSION

SCs migrate and divide along peripheral axons and the intimate contact between the two contributes to SC proliferation, mainly through the neuregulin/ErbB axis. Other signals provided by ECM proteins are also important for their proliferation (Lyons et al., 2005; Bunge et al., 1982; 1990; Michailov et al., 2004; Nave and Salzer, 2006). Here, we investigated the characteristics of SC division and its impact on myelination in zebrafish.
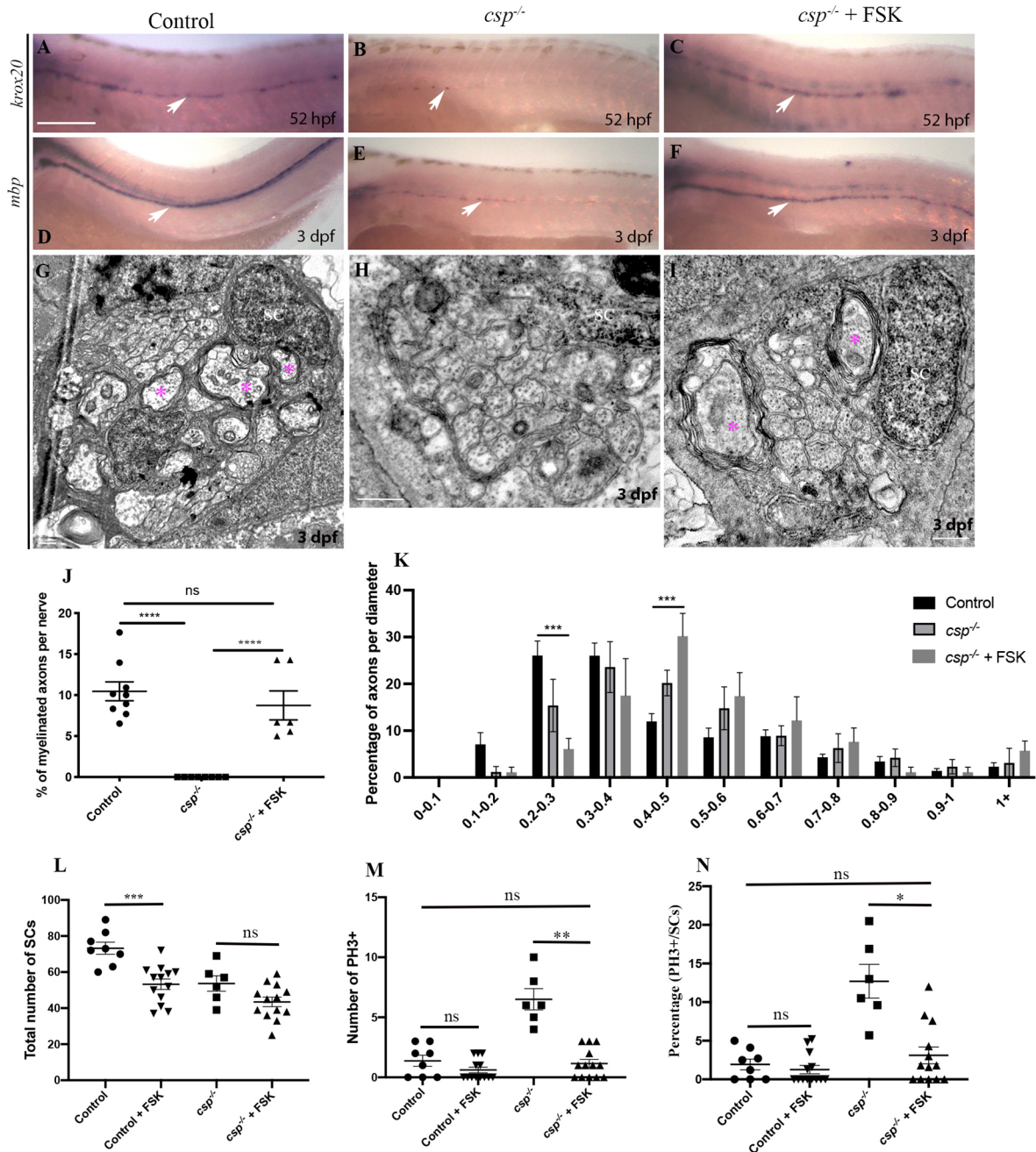
Fig. 5. *sil* is required to initiate myelin gene expression and axonal wrapping by SCs via a cAMP-dependent pathway. (A-C) Lateral views of *krox20* expression at 52 hpf revealed by *in situ* hybridization along the PLLn in control (A) showing a robust expression (*n*=29 embryos), *csp*^{−/−} embryo (B) showing a sharp decrease in *krox20* expression (*n*=22 embryos) and in *csp*^{−/−} treated with FSK (C) showing a robust expression similar to controls (*n*=30 embryos). Arrows indicate SCs expressing *krox20* along the PLLn. (D-F) Lateral views of *mbp* expression at 3 dpf revealed by *in situ* hybridization along the PLLn in control (D) showing a robust expression (*n*=31 embryos), *csp*^{−/−} embryo (E) showing a sharp decrease in *mbp* expression (*n*=24 embryos) and in *csp*^{−/−} treated with FSK (F) showing a robust expression similar to controls (*n*=28 embryos). Arrows indicate SCs expressing *mbp* along the PLLn. Scale bar: 200 μm. (G-I) TEM of a cross-section of the PLLn at 3 dpf in control (G), *csp*^{−/−} (H) and *csp*^{−/−} treated with FSK between 45 and 52 hpf (I). Magenta asterisks indicate some large caliber myelinated axons. Scale bars: 0.5 μm. (J) Quantification of the percentage of myelinated axons relative to the total number of axons per nerve at 3 dpf in controls (average of 10.6±1.17), *csp*^{−/−} (average of 0) and *csp*^{−/−} treated with FSK (average of 8.74±1.77, six nerves, *n*=5 embryos) (****$P \leq 0.0001$; ns, $P=0.4846$). (K) Graph representing the distribution of axons relative to their diameter with 0.1 μm bin width at 3 dpf in controls, *csp*^{−/−} and *csp*^{−/−} embryos treated with FSK (***$P=0.0001$ for 0.2-0.3; ***$P=0.0007$ for 0.4-0.5). (L) Quantification of the number of SCs within a defined region of the PLLn at 54 hpf in control (average of 73.25±3.36 cells, *n*=8 embryos), control treated with FSK (average of 53.23±2.89 cells, *n*=13 embryos), *csp*^{−/−} (average of 53.68±4.28, *n*=6 embryos) and *csp*^{−/−} treated with FSK (average of 43.46±2.65 cells, *n*=13 embryos). (***$P=0.0005$; ns, $P=0.27$). (M) Quantification of the number of PH3⁺ SCs within a defined region of the PLLn at 54 hpf in control (average of 1.37±0.46 cells, *n*=8 embryos), control treated with FSK (average of 0.61±0.24 cells, *n*=13 embryos), *csp*^{−/−} (average of 6.50±0.88 cells, *n*=6 embryos) and *csp*^{−/−} treated with FSK (average of 1.15±0.33 cells, *n*=13 embryos) (ns, $P>0.9999$; **$P=0.004$). (N) Quantification of the percentage of PH3⁺ SCs relative to the total number of SCs within a defined region of the PLLn at 54 hpf in control (average of 1.93±0.69 cells, *n*=8 embryos), control treated with FSK (average of 1.26±0.54 cells, *n*=13 embryos), *csp*^{−/−} (average of 12.70±2.17 cells, *n*=6 embryos) and *csp*^{−/−} treated with FSK (average of 3.10±1.07 cells, *n*=13 embryos) (ns, $P>0.9999$; *$P=0.018$).
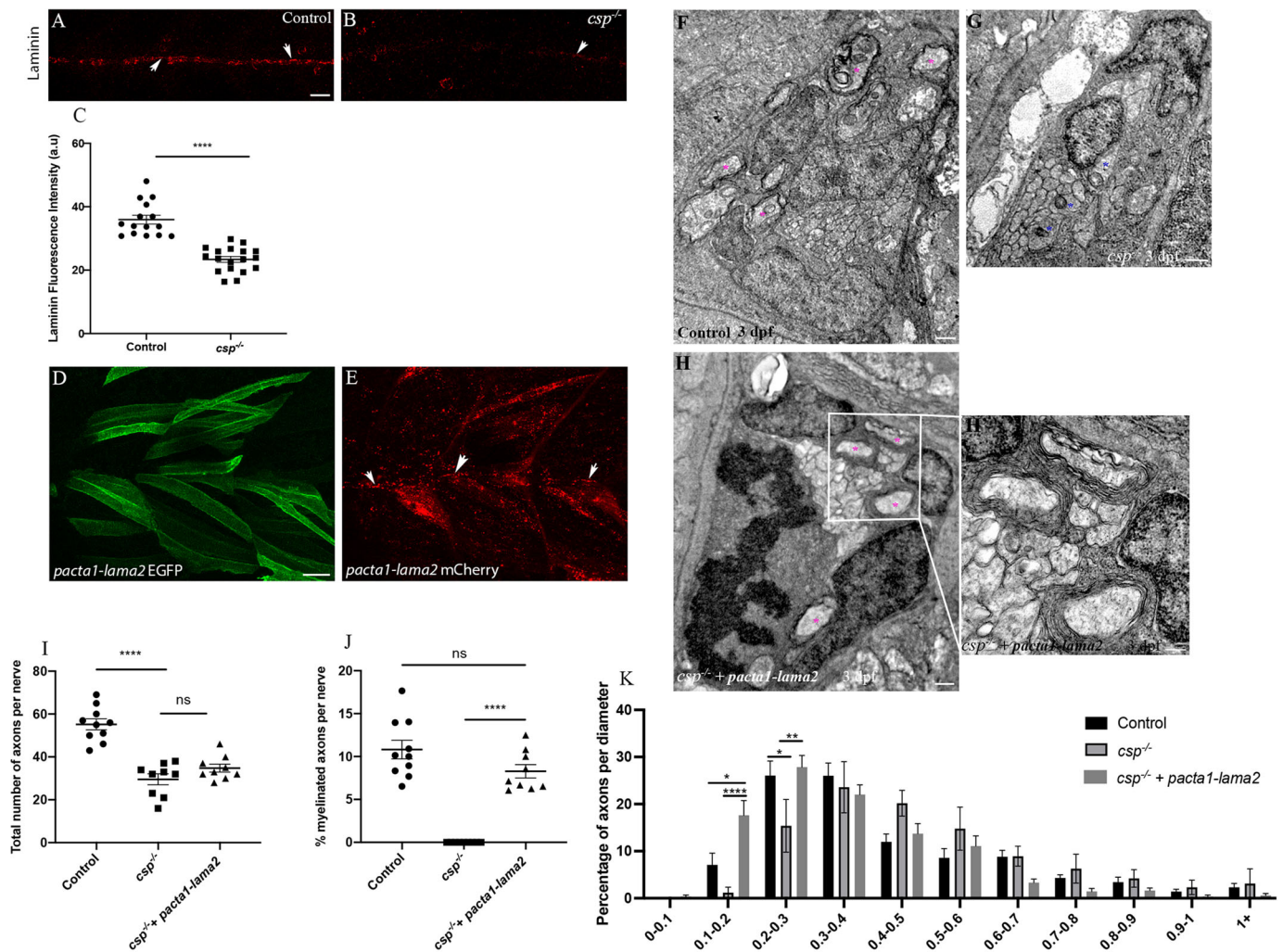
Fig. 6. Laminin expression is significantly reduced in $csp^{-/-}$ and Laminin $\alpha 2$ overexpression rescues radial sorting and myelination defects in $csp^{-/-}$ embryos. (A,B) Laminin expression in control (A) and $csp^{-/-}$ (B) embryos at 48 hpf showing the PLLn nerve (arrows). Scale bar: 20 μm. (C) Quantification of laminin fluorescence intensity along the PLLn in controls (average of 35.95±1.39, n=15 embryos) and $csp^{-/-}$ (average of 23.37±0.90, n=18 embryos) embryos at 48 hpf (****$P \leq 0.0001$, a.u., arbitrary unit. (D) Lateral view of EGFP expression in muscles surrounding the PLLn following *pacta1-lama2* injection. Scale bar: 20 μm. (E) Lateral view of mCherry-tagged secreted laminin in muscles and within the PLLn (white arrows). (F-H′) TEM of a cross-section of the PLLn at 3 dpf in control (F), $csp^{-/-}$ (G) and $csp^{-/-}$+*pacta1-lama2* (H) embryos. Magenta asterisks indicate some large caliber myelinated axons; some are shown at higher magnification in H′. Scale bars: 0.5 μm. (I) Quantification of the total number of axons per nerve at 3 dpf in controls (average of 55.20±2.56, ten nerves, n=6 embryos), $csp^{-/-}$ (average of 29.56±2.55, nine nerves, n=7 embryos) and $csp^{-/-}$+*pacta1-lama2* (average of 34.78±1.84, nine nerves, n=7 embryos) (****$P \leq 0.0001$; ns, P=0.1190). (J) Quantification of the percentage of myelinated axons relative to the total number of axons per nerve at 3 dpf in controls (average of 10.82±1.085), $csp^{-/-}$ (average of 0±0) and $csp^{-/-}$+*pacta1-lama2* (average of 8.28±0.77) (****$P \leq 0.0001$; ns, P=0.075). (K) Graph representing the distribution of axons relative to their diameter with 0.1 μm bin width at 3 dpf in controls, $csp^{-/-}$ and $csp^{-/-}$ injected with *pacta1-lama2* (*P=0.033 for 0.1-0.2; *P=0.04 for 0.2-0.3; **P=0.005; ****P<0.0001).

SCs must regulate their numbers in order to myelinate or ensheath all axons that are supposed to be myelinated by the end of radial sorting (Jessen and Mirsky, 2005), so one would predict that reducing the number of SCs in the nerve would result in a reduction of myelinated axons. Indeed, several molecules that control SC proliferation have been identified, such as Cdc42, focal adhesion kinase and several extracellular matrix proteins of the laminin family such as laminins 2, 8 and γ1 (Benninger et al., 2007; Grove et al., 2007; Yang et al., 2005). Specific ablation of these molecules in SCs causes a reduction in the number of myelinated axons.

But, how important is the timely division of SC? Are insufficient SC numbers per se a cause of radial sorting and myelination defects?

Here, we show that timely SC division is essential for peripheral radial sorting and myelination. Delaying SC division during development is sufficient to halt radial sorting and axonal ensheathment (Fig. 9). We provide evidence that laminin expression is significantly reduced along the PLLn in embryos with delayed SC division. Providing laminin, through surrounding muscles or from within SCs, which reduces even further the number of SCs and their proliferation, is enough to initiate radial sorting and myelination (Fig. 9). Several studies have pointed to a role for laminin in controlling SC proliferation, but this is the first study that implicates SC division in laminin expression and subsequent myelination. The temporal control of SC division is therefore an important step towards initiating the myelination program through the laminin/cAMP pathway, a role that stretches beyond simply increasing the pool of SCs required to
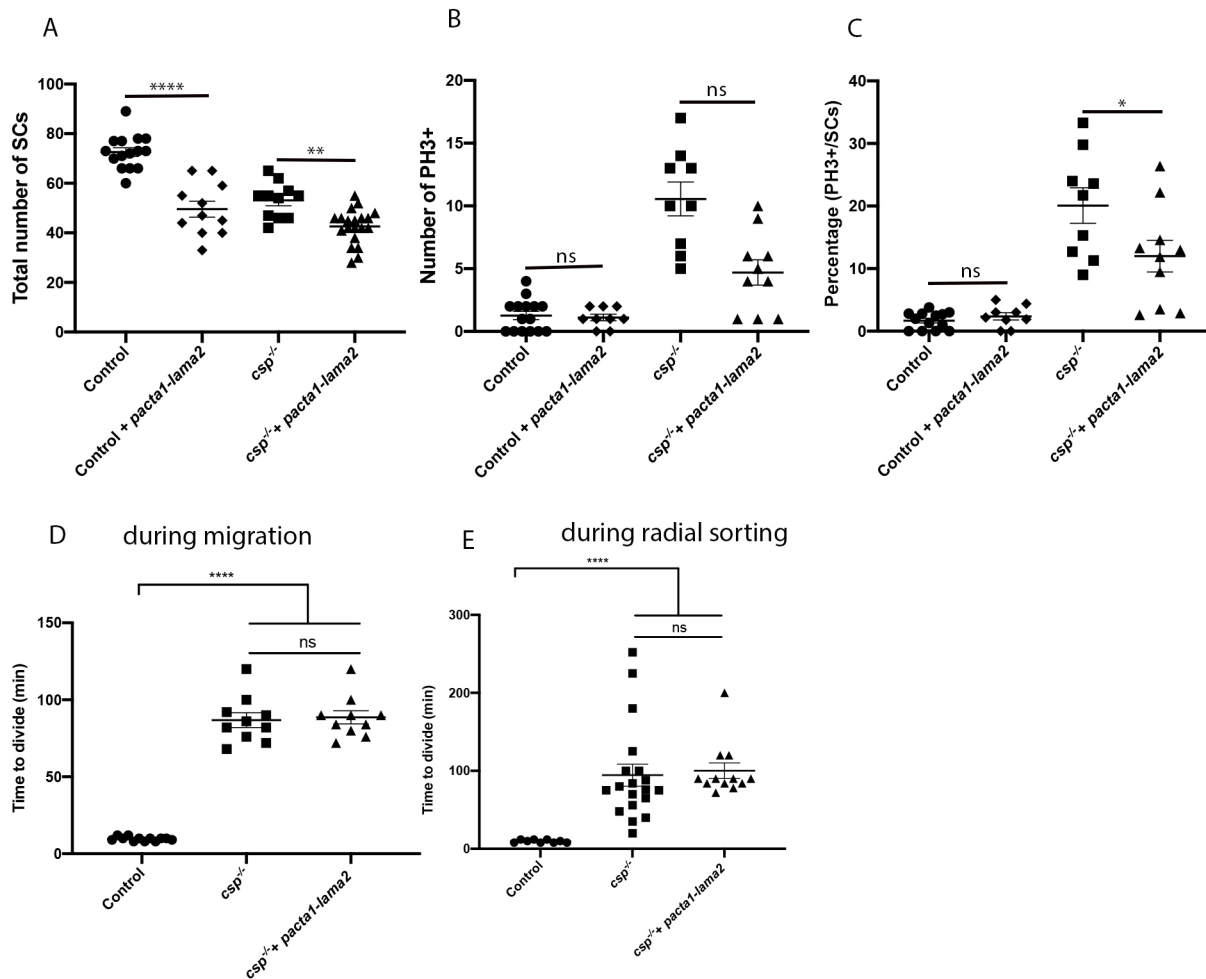
Fig. 7. Laminin α2 overexpression reduces the number of SCs in controls and *csp*−/− embryos. (A) Quantification of the number of SCs within a defined region of the PLLn at 48 hpf in control (average of 72.60±1.78 cells, *n*=15 embryos), control injected with *pacta1-lama2* (average of 49.55±3.18 cells, *n*=11 embryos), *csp*−/− (average of 53.09±2.15, *n*=11 embryos) and *csp*−/− injected with *pacta1-lama2* (average of 42.60±1.56 cells, *n*=20 embryos) (****P<0.0001; **P=0.004). (B) Quantification of the number of PH3+ SCs within a defined region of the PLLn at 48 hpf in control (average of 1.26±0.36 cells, *n*=15 embryos), control injected with *pacta1-lama2* (average of 1.11±0.26 cells, *n*=9 embryos), *csp*−/− (average of 10.56±1.34 cells, *n*=9 embryos) and *csp*−/− injected with *pacta1-lama2* (average of 4.70±1.01 cells, *n*=10 embryos) (ns, *P*>0.9999, control versus control+*pacta1-lama2*; ns, *P*=0.28, *csp*−/− versus *csp*−/−+*pacta1-lama2*). (C) Quantification of the percentage of PH3+ SCs relative to the total number of SCs within a defined region of the PLLn at 48 hpf in control (average of 1.68±0.38 cells, *n*=13 embryos), control injected with *pacta1-lama2* (average of 2.36±0.57 cells, *n*=9 embryos), *csp*−/− (average of 20.08±2.83 cells, *n*=9 embryos) and *csp*−/− injected with *pacta1-lama2* (average of 11.99±2.51 cells, *n*=10 embryos) (ns, *P*>0.9999; *P=0.022). (D) Quantification of the time required for control (average of 9.66±0.39, 12 cells, *n*=4 embryos), *csp*−/− (average of 86.80±4.77, ten cells, *n*=4 embryos) and *csp*−/− injected with *pacta1-lama2* (average of 88.60±4.31, ten cells, *n*=4 embryos) SCs to successfully complete cytokinesis during migration (****P≤0.0001; ns, *P*=0.7828). (E) Quantification of the time required for control (average of 9.77±0.61, nine cells, *n*=4 embryos), *csp*−/− (average of 94.42±14.18, 19 cells, *n*=4 embryos) and *csp*−/− injected with *pacta-lama2* (average of 100.2±10.01, 12 cells, *n*=4 embryos) SCs to successfully complete cytokinesis during radial sorting (****P≤0.0001; ns, *P*=0.1424).

continuously engulf the nerve as it grows. Consequently, is it important to generate enough SCs for myelination to proceed? Our findings reveal that the myelination defects observed in *csp*−/− embryos do not ensue from the reduction in SC numbers per se, because laminin overexpression can fully rescue the percentage of myelinated axons within the PLLn even if SC numbers remain significantly reduced. Indeed, laminin overexpression and FSK treatment restore myelination in *csp*−/− mutants while reducing even further the number of SCs and/ or their proliferation. This points to a role for laminin/cAMP in prompting myelination by interrupting proliferation and that this pathway does not drive proliferation in order to myelinate. Nonetheless, it is important to note that different levels of laminin/ cAMP expression or activity may coordinate SC proliferation and differentiation during development.

Given that *csp*−/− embryos show a radial sorting defect, it remains possible that the myelination defects result, at least partially, from defective cytoskeletal re-arrangement. A group of genes that regulate this aspect of SC behavior has been identified and includes *elmo1*, *dock1*, β1 integrin genes and *ILK*, which link extracellular signaling to *rac1* (Mikdache et al., 2020; Cunningham et al., 2018; Feltri et al., 2002). Our analysis strongly suggests that the myelination defects observed in *csp*−/− do not result from defective Rac1 activity as forcing the expression of Rac1 does not rescue this defect, even partially.

SCs in *csp*−/− struggle to progress through the M phase of the cell cycle. This phase is characterized by chromatin condensation and by ejection of transcription factors and chromatin-binding proteins (Ma et al., 2015). It is possible that SC transcription factors
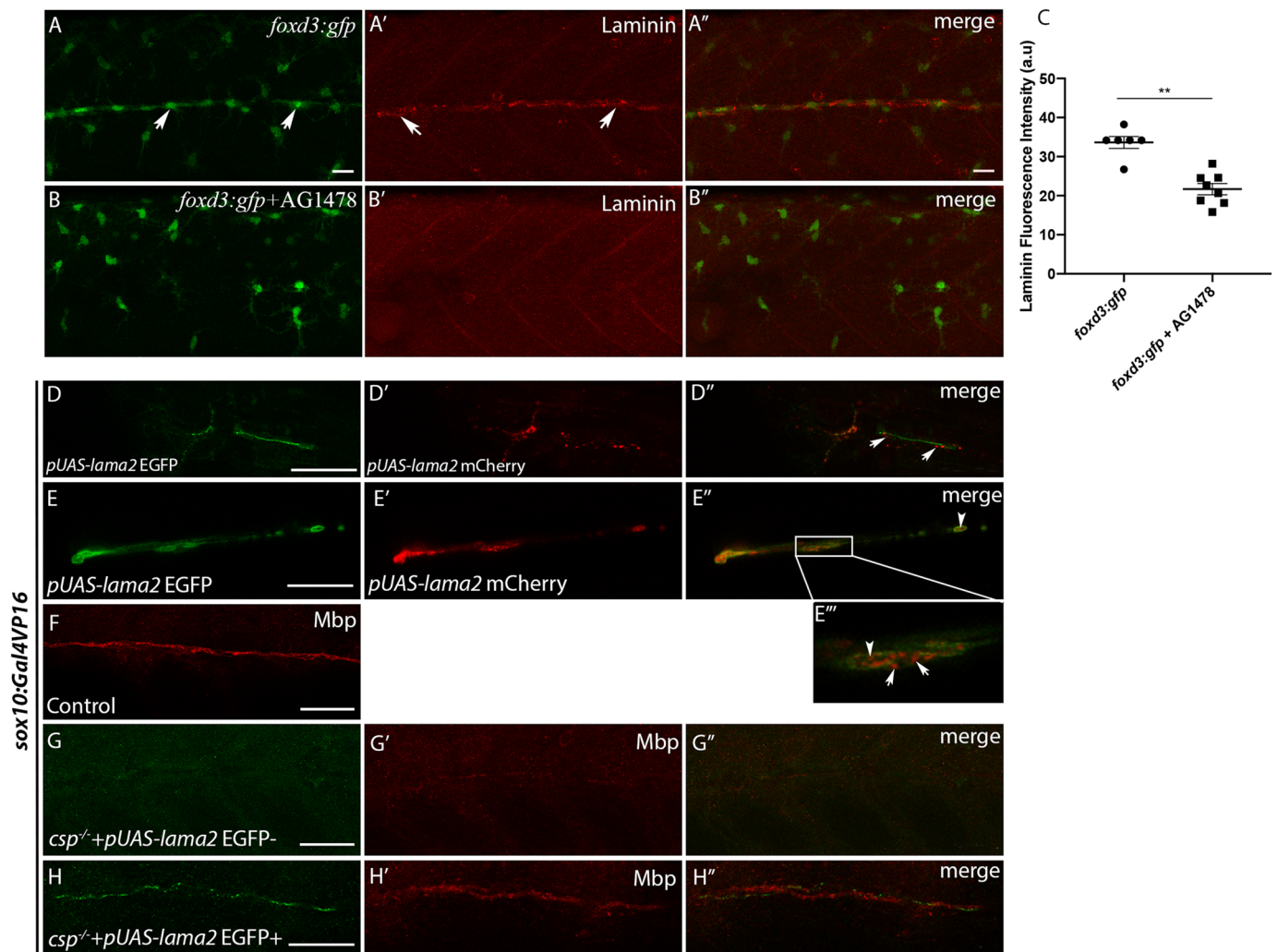
DEVELOPMENT

10

Fig. 8. Laminin expression is significantly reduced in AG1478-treated embryos and Laminin α2 overexpression within SCs restores normal Mbp expression in $csp^{-/-}$ embryos. (A-B″) Laminin immunostaining in *foxd3:gfp* (A-A″) and *foxd3:gfp* embryos treated with AG1478 (B-B″) at 48 hpf. Arrows indicate GFP$^+$ SCs in A and laminin expression along the PLLn in A′. Scale bars: 20 μm. A″ and B″ are the merge images of A and A′ and of B and B′, respectively. (C) Quantification of laminin fluorescence intensity along the PLLn in *foxd3:gfp* (average of 33.63±1.52, *n*=6 embryos) and *foxd3:gfp*/AG1478-treated (average of 21.67±1.44, *n*=8 embryos) embryos (**P=0.0013), a.u., arbitrary unit. (D,E) Lateral views of EGFP expression in SCs of the PLLn following *pUAS-lama2* injection in *sox10:Gal4VP16* embryos. Scale bars: 20 μm. (D′,E′) Lateral views of mCherry-tagged secreted laminin in SCs and within the PLLn. (D″,E″) Merge of D and D′ and of E and E′, respectively. mCherry-tagged secreted laminin is highlighted in E‴ at higher magnification; white arrows in D″ and E‴ indicate extracellular laminin within the PLLn and white arrowheads in E″ and E‴ indicate mCherry-tagged laminin within SCs. (F) Lateral view of Mbp immunolabeling in control embryo at 3 dpf. Scale bar: 50 μm. (G,G′) Lateral view showing the absence of EGFP expression in SCs of the PLLn (G) that correlates with a significant decrease in Mbp immunolabeling (G′) following *pUAS-lama2* injection but with no EGFP/mCherry expression in $csp^{-/-}$/*sox10:Gal4VP16* embryos. *n*=24. Scale bar: 50 μm. (G″) Merge of G and G′. (H,H′) Lateral view showing EGFP expression in SCs of the PLLn that correlates with normal Mbp immunolabeling (H′) following *pUAS-lama2* injection with positive clones of EGFP/mCherry in $csp^{-/-}$/*sox10:Gal4VP16* embryos. *n*=8. Scale bar: 20 μm. (H″) Merge of H and H′.

required for the initiation of myelination are permanently ejected in $csp^{-/-}$ and therefore unable to bind the DNA. Another possibility is defective upstream signaling activity in $csp^{-/-}$ embryos that blocks SC differentiation, assuming that chromatin accessibility is re-established after division. Our analysis suggests that it is rather defective signaling activity that is responsible for the peripheral lack of myelin observed in $csp^{-/-}$ embryos and that transcription activity is responsive to upstream signaling cues.

A particularly interesting observation is the difference in the *sil* deficiency phenotype between retina and Schwann cells. Sil is a ubiquitously expressed protein and is involved in the fundamental process of mitosis but is highly enriched in the nervous system. Neurons might in this case be more sensitive to Sil defects leading to

massive apoptosis within the central nervous system; however, it is Schwann cell differentiation that is impaired in $csp^{-/-}$ with no increase in apoptosis. It is therefore possible that different cells might respond differently to *sil* defects and our results suggest that genes involved in MCPH have a broader requirement during development that is not solely confined to neuronal cells in the central nervous system.

What is the molecular link between SC division, its temporal control and the cAMP pathway? Several studies have now established an essential role for the Gpr126 (*adgrg6*) in driving cAMP activity in SC through G proteins (Mogha et al., 2013) and this has recently been attributed to an interaction of Gpr126 with the ECM, more specifically with Laminin 211 (Petersen et al., 2015). It is therefore
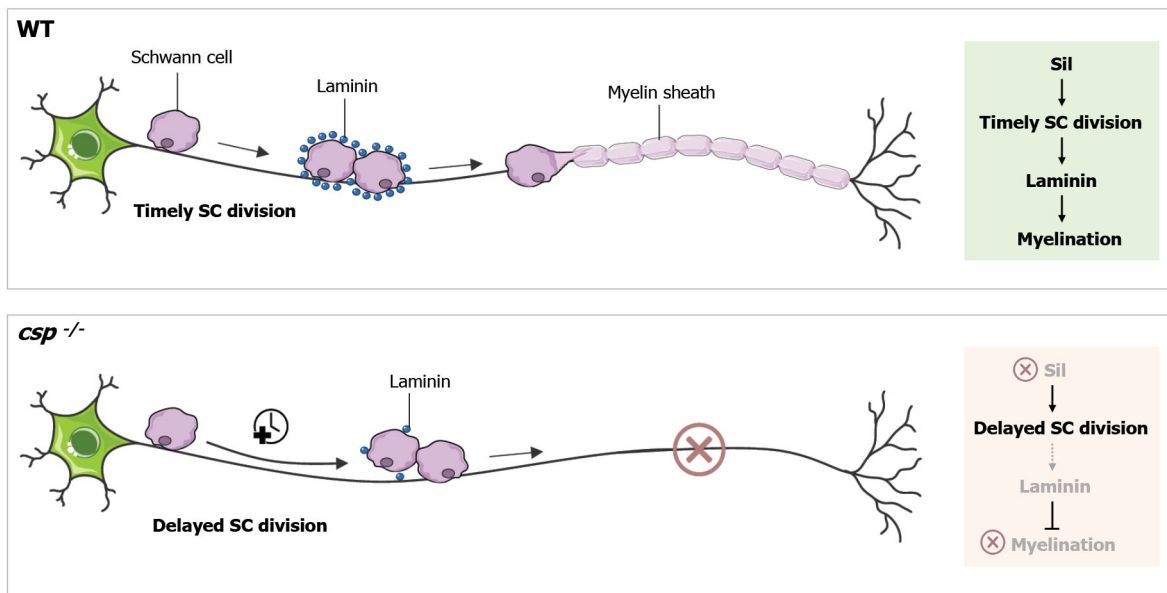
Fig. 9. Model for *sil* function in SC radial sorting and myelination. The data presented here support a model in which Sil controls the timely division of SCs. Sil function is required for laminin expression in order to drive radial sorting and myelination. In the absence of Sil, laminin expression is significantly reduced, resulting in defective radial sorting and a complete loss of SC myelination. WT, wild type.

possible that *sil*-deficient SCs are incapable of secreting extracellular proteins and/or responding to them to drive the ECM/Gpr126/cAMP pathway (Paavola et al., 2014; Petersen et al., 2015). Our work strongly suggests that timely SC division is required for timely laminin expression. Laminin, in return, with increasing levels and polymerization, would drive radial sorting and myelination through cAMP activation, at least partially via Gpr126 (Petersen et al., 2015).

Finally, we show that SCs are a major source of laminin within peripheral nerves in zebrafish. Our clonal analysis shows that forcing laminin expression autonomously within SCs is enough to lead to secretion of laminin into the extracellular space and restore normal Mbp expression within the vicinity of these cells in *csp*−/− embryos.

In summary, our work provides evidence of a previously unappreciated mechanism that links temporal control of SC division to radial sorting and axonal wrapping via the laminin/cAMP pathway *in vivo*.

MATERIALS AND METHODS
Embryo care
Zebrafish (*Danio rerio*) of the AB strain were used. Embryos were staged and cared for according to standard protocols (https://zfin.org/zf_info/zfbook/cont.html). The stable transgenic line *Tg(foxd3:gfp)*, which labels SCs, was used in this study (Gilmour et al., 2002). The *Tg(sox10: Gal4VP16)el159* line was kindly provided by Gage Crump (Center for Stem Cell and Regenerative Medicine, Keck School of Medicine, University of Southern California, Los Angeles, CA, USA). *Csp+/−* embryos (*stilcz65*) were purchased from the Zebrafish International Resource Center (ZIRC). All animal experiments were conducted with approved protocols at Inserm by DDPP Val de Marne, France, under license number F 94-043-013.

Plasmid constructs
pTol2-Sox10:Sil-P2A-mCherry
The sil-P2A-mCherry cassette, which allows simultaneous expression of *sil* and membrane-localized mCherry separated by the self-cleaving P2A peptide, was generated by PCR amplification.

5′-CGATTCACTAGTATGAACCGTGTACAAGTGGATTTTAAAGG-3′ (forward) and 5′-GAAGTTCGTGGCTCCGGATCCAAAGAGCTTG-GGGAGCTGCCGTAACC-3′ (reverse) primers were used on the pDNR-lib-STIL cDNA (Horizon Discovery, MDR1734-202835545) and the 5′-GGTTACGGCAGCTCCCCAAGCTCTTTGGATCCGGAGCCACGA-ACTTC-3′ (forward) and 5′-CTATGACCATGATTACGCCAAG-3′ (reverse) primers on the pCS2-mCherry-CAAX plasmid.

The resulting PCR fragment was digested by SpeI and NotI before subcloning into the −4725Sox10-cre vector (a gift from Robert Kelsh, Centre for Regenerative Medicine, Developmental Biology Programme, School of Biology and Biochemistry, University of Bath, UK) to obtain the *pSox10:sil-P2A-mCherry* plasmid.

p5UAS: lama2-mCherry-T2A-EGFPcaax
pT2i5uasbiH2bChe-GFP (a gift from Michel Volovitch, Centre Interdisciplinaire de Recherche en Biologie, Collège de France, Paris, France) was used to amplify the 5′ UAS sequence using 5′-GT-GGGCCCTGCGTCTAGAGTC-3′ (forward) and 5′-CTACCATATG-GGCGACCGGTGG-3′ (reverse) primers. Then, in order to replace the *acta1* promoter, the PCR product was subcloned into the *pacta1: lama2-mCherry-T2A-EGFPcaax* vector [a gift from Peter Currie (Australian Regenerative Medicine Institute, Monash University, Clayton, Australia) and Kelly Monk (The Vollum Institute, Oregon Health & Science University, Portland, OR, USA)] digested with ApaI and NdeI enzymes.

Microinjections
Mito:gfp (a gift from Dominik Paquet, Institute for Stroke and Dementia Research, and SyNergy, Ludwig-Maximilians University, Munich, Germany) and *h2b::gfp* (a gift from Jon Clarke, Department of Developmental Neurobiology, King's College London, UK) mRNAs were synthesized using the SP6 mMessage mMachine System after linearization with NotI and injected at 200 pg per embryo. *pTol2:sox10-sil-2A-mCherry-Caax* was injected at 10 pg per embryo along with 50 pg of *tol2* transposase mRNA (a gift from David Lyons, Centre for Discovery Brain Sciences, University of Edinburgh, UK). *Rac1V12* (constitutively active Rac1, kindly provided by Nicolas David, Laboratory for Optics and Biosciences, Institut Polytechnique de Paris, Palaiseau, France) mRNA was synthesized using the SP6 mMessage mMachine System after linearization with NotI and injected at 2-10 pg per embryo. *pacta1-lama2* (kindly provided by Kelly Monk and Peter Currie) was injected at 20 pg per embryo along with 100 pg of Tol2 transposase mRNA. *pUAS-lama2* was injected at 20 pg per embryo.

In situ hybridization

In situ hybridization was performed following standard protocols using *krox20* and *mbp* probes (Fontenas et al., 2016). Embryos were raised in egg water with phenylthiourea (0.003%) to avoid pigmentation and were fixed overnight in 4% paraformaldehyde (PFA) at 52 hpf and 3 dpf. Embryos were dehydrated the next day and kept in methanol at −20°C. Embryos were then rehydrated and treated with proteinase K and incubated overnight with the corresponding probe. Embryos were then washed and the staining was revealed using anti-digoxigenin antibody (Roche; 11093274910).

Immunofluorescence

The following antibodies and dilutions were used: mouse anti-acetylated tubulin (Sigma-Aldrich; 1/500; T7451), mouse anti-HuC/HuD neuronal protein (Invitrogen; 1/500; A21271), rabbit anti-laminin (Sigma-Aldrich, 1/200; L9393), mouse anti-phospho histone 3 (Ser 10) (Millipore; 1/500; 06-570), rabbit anti-myelin basic protein (custom produced; Tingaud-Sequeira Angèle et al., 2017; gift from Patrick Babin, Laboratoire Maladies Rares: Génétique et Métabolisme, Université de Bordeaux, France; 1/500), mouse anti-EGFP (Millipore; 1/500; MAB3580). Primary antibodies were detected with appropriate secondary antibodies conjugated to either Alexa 488, Alexa 568 or Alexa 647 (Invitrogen; A11036, A11034, A11001 and A31571) at 1/500. For immunostaining, embryos were fixed in 4% PFA in 1× PBS overnight at 4°C, then washed with 1× PBS and dehydrated in methanol for at least 6 h at −20°C. Samples were then rehydrated, digested with proteinase K and blocked with 0.5% Triton X-100 in PBS and 10% sheep serum and then incubated with primary antibody overnight at 4°C (diluted in PBS with 2% sheep serum). Larvae were then washed with PBS for a few hours and then incubated with secondary antibody in 0.5% Triton X-100 in PBS and 2% sheep serum overnight at 4°C. Stained larvae were then imaged with a Leica SP8 confocal microscope. For laminin and Mbp staining, embryos were fixed in 4% PFA for 30 min and treated for 7 min with acetone at −20°C. Samples were then blocked with 0.5% Triton X-100 in PBS and 10% sheep serum and then incubated with primary antibody overnight at 4°C (diluted in PBS with 2% sheep serum). Larvae were then washed with PBS for a few hours and then incubated with secondary antibody in 0.5% Triton X-100 in PBS and 2% sheep serum for 3 h at room temperature. For laminin fluorescence intensity quantification, the same parameters (excitation/emission, gain for detectors, lasers intensity) were applied for image acquisition in controls and $csp^{-/-}$ embryos, and fluorescence intensity was measured using ImageJ ('Analyze/measure').

Forskolin and AG1478 treatment

Embryos were incubated in fish water containing 20 μM FSK diluted in DMSO between 45 and 52 hpf. Controls were incubated in the equivalent amount of DMSO solution (0.1%) during the same period.

Embryos were incubated in fish water containing 4 μM AG1478 diluted in DMSO between 24 and 48 hpf. Controls were incubated in the equivalent amount of DMSO solution (0.1%) during the same period.

Acridine Orange staining

Embryos were anesthetized with 0.03% tricaine and incubated in fish water containing 5 μM Acridine Orange for 20 min in the dark. After washing, they were embedded in 1.5% low melting point agarose, and imaged with a Leica SP8 confocal microscope. Transmitted light imaging was used to identify the PLLn and the spinal cord for counting apoptotic corpses within these structures. Fluorescent corpses were counted at the level of the yolk extension.

Schwann cell and PH3^{+} SC cell counts

Tg(foxd3:gfp) embryos, $csp^{-/-}/Tg(foxd3:gfp)$ as well as treated and injected ones were analyzed. Schwann cells and PH3^{+} SCs were counted from the most anterior to the end of the yolk extension along the AP axis (≈900 μm) after immunostaining. Schwann cells as well as PH3^{+} SCs were counted blindly by two independent researchers using ImageJ.

Neuronal cell counting

Total neuronal cell numbers (HuC[+]) were counted from a confocal *z*-series of the PLLg using ImageJ (Mikdache et al., 2021). Cells were counted blindly by two independent researchers.

Live imaging

Embryos were anesthetized with 0.03% tricaine and embedded in 1.5% low melting point agarose. For *mito:GFP* tracking experiments, the PLLn was examined at 48 hpf from a lateral view. A series of 10 min time-lapses recordings were made. Recordings were performed at 27°C using a Leica SP8 confocal microscope. For *Tg(foxd3:gfp)*, $Tg(foxd3:gfp)/csp^{-/-}$ as well as controls and $csp^{-/-}$ injected and treated embryos, the PLLn was examined at different time points and recordings were acquired for up to 12 h. Transmitted light imaging was used to identify the PLLn for *h2b:gfp* and *mito:GFP* recordings.

TEM

At 3 and 4 dpf, embryos were fixed in a solution of 2% glutaraldehyde, 2% PFA and 0.1 M sodium cacodylate, pH 7.3, overnight at 4°C. This was followed by a post-fixation step in cacodylate-buffered 1% osmium tetroxide (Serva) for 1 h at 4°C and in 2% uranyl acetate for 1 h at room temperature. The tissue was then dehydrated and embedded in epoxy resin. Sections were contrasted with saturated uranyl acetate solution and were examined with a 1010 electron microscope (JEOL) and a digital camera (Gatan).

Statistical analysis

Means and standard errors of the mean were calculated with Graph Pad Prism 7. All data were first tested for normal distribution using the Shapiro–Wilk normality test combined with D'Agostino & Pearson normality test. All experiments with only two groups and one dependent variable were compared using an unpaired *t*-test with Welch's correction if they passed normality test; if not, groups were compared with the nonparametric Mann–Whitney test. Statistically significant differences were determined using one-way ANOVA for all experiments with more than two groups but only one dependent variable if data were normally distributed; if not, groups were compared using Kruskal–Wallis test. Error bars depict s.e.m. In figures, the following notation is used to represent significance levels: ns, not significant ($P>0.05$); *$P≤0.05$; **$P≤0.01$; ***$P≤0.001$; ****$P≤0.0001$. *n* represents the number of embryos.

References

Aplan, P. D., Lombardi, D. P., Ginsberg, A. M., Cossman, J., Bertness, V. L. and Kirsch, I. R. (1990). Disruption of the human SCL locus by "illegitimate" V-(D)-J recombinase activity. *Science* 250, 1426-1429. doi:10.1126/science.2255914

Aplan, P. D., Lombardi, D. P. and Kirsch, I. R. (1991). Structural characterization of SIL, a gene frequently disrupted in T-cell acute lymphoblastic leukemia. *Mol. Cell. Biol.* 11, 5462-5469. doi:10.1128/mcb.11.11.5462-5469.1991

Benninger, Y., Thurnherr, T., Pereira, J. A., Krause, S., Wu, X., Chrostek-Grashoff, A., Herzog, D., Nave, K. A., Franklin, R. J., Meijer, D. et al. (2007). Essential and distinct roles for cdc42 and rac1 in the regulation of Schwann cell

biology during peripheral nervous system development. *J. Cell Biol.* **177**, 1051-1061. doi:10.1083/jcb.200610108

Bouçanova, F. and Chrast, R. (2020). Metabolic interaction between Schwann cells and axons under physiological and disease conditions. *Front. Cell Neurosci.* **14**, 148. doi:10.3389/fncel.2020.00148

Boueid, M. J., Mikdache, A., Lesport, E., Degerny, C. and Tawk, M. (2020). Rho GTPases signaling in zebrafish development and disease. *Cells* **9**, 2634. doi:10.3390/cells9122634

Bunge, M. B., Williams, A. K. and Wood, P. M. (1982). Neuron-Schwann cell interaction in basal lamina formation. *Dev. Biol.* **92**, 449-460. doi:10.1016/0012-1606(82)90190-7

Bunge, M. B., Clark, M. B., Dean, A. C., Eldridge, C. F. and Bunge, R. P. (1990). Schwann cell function depends upon axonal signals and basal lamina components. *Ann. N. Y. Acad. Sci.* **580**, 281-287. doi:10.1111/j.1749-6632.1990.tb17937.x

Campaner, S., Kaldis, P., Izraeli, S. and Kirsch, I. R. (2005). Sil phosphorylation in a Pin1 binding domain affects the duration of the spindle checkpoint. *Mol. Cell. Biol.* **25**, 6660-6672. doi:10.1128/MCB.25.15.6660-6672.2005

Chen, Z.-L. and Strickland, S. (2003). Laminin γ1 is critical for Schwann cell differentiation, axon myelination, and regeneration in the peripheral nerve. *J. Cell Biol.* **163**, 889-899. doi:10.1083/jcb.200307068

Chernousov, M. A., Yu, W. M., Chen, Z. L., Carey, D. J. and Strickland, S. (2008). Regulation of Schwann cell function by the extracellular matrix. *Glia* **56**, 1498-1507. doi:10.1002/glia.20740

Colognato, H. and Tzvetanova, I. D. (2011). Glia unglued: how signals from the extracellular matrix regulate the development of myelinating glia. *Dev. Neurobiol.* **71**, 924-955. doi:10.1002/dneu.20966

Court, F. A., Hewitt, J. E., Davies, K., Patton, B. L., Uncini, A., Wrabetz, L. and Feltri, M. L. (2009). A laminin-2, dystroglycan, utrophin axis is required for compartmentalization and elongation of myelin segments. *J. Neurosci.* **29**, 3908-3919. doi:10.1523/JNEUROSCI.5672-08.2009

Cunningham, R. L., Herbert, A. L., Harty, B. L., Ackerman, S. D. and Monk, K. R. (2018). Mutations in dock1 disrupt early Schwann cell development. *Neural. Dev.* **13**, 17. doi:10.1186/s13064-018-0114-9

Eldridge, C. F., Bunge, M. B. and Bunge, R. P. (1989). Differentiation of axon-related Schwann cells in V&O:II. Control of myelin formation by basal lamina. *J. Neurosci.* **9**, 625-638. doi:10.1523/JNEUROSCI.09-02-00625.1989

Feltri, M. L., Graus Porta, D., Previtali, S. C., Nodari, A., Migliavacca, B., Cassetti, A., Littlewood-Evans, A., Reichardt, L. F., Messing, A., Quattrini, A. et al. (2002). Conditional disruption of β1 integrin in Schwann cells impedes interactions with axons. *J. Cell Biol.* **156**, 199-210. doi:10.1083/jcb.200109021

Feltri, M. L., Poitelon, Y. and Previtali, S. C. (2016). How Schwann cells sort axons: new concepts. *Neuroscientist* **22**, 252-265. doi:10.1177/1073858415572361

Fontenas, L., De Santis, F., Di Donato, V., Degerny, C., Chambraud, B., Del Bene, F. and Tawk, M. (2016). Neuronal Ndrg4 is essential for nodes of Ranvier organization in zebrafish. *PLoS Genet.* **12**, e1006459. doi:10.1371/journal.pgen.1006459

Gilmour, D. T., Maischein, H. M. and Nüsslein-Volhard, C. (2002). Migration and function of a glial subtype in the vertebrate peripheral nervous system. *Neuron* **34**, 577-588. doi:10.1016/S0896-6273(02)00683-9

Grove, M., Komiyama, N. H., Nave, K. A., Grant, S. G., Sherman, D. L. and Brophy, P. J. (2007). FAK is required for axonal sorting by Schwann cells. *J. Cell Biol.* **176**, 277-282. doi:10.1083/jcb.200609021

Hara, M. and Fukagawa, T. (2020). Dynamics of kinetochore structure and its regulations during mitotic progression. *Cell. Mol. Life Sci.* **77**, 2981-2995. doi:10.1007/s00018-020-03472-4

Herbert, A. L. and Monk, K. R. (2017). Advances in myelinating glial cell development. *Curr. Opin. Neurobiol.* **42**, 53-60. doi:10.1016/j.conb.2016.11.003

Jessen, K. R. and Mirsky, R. (2005). The origin and development of glial cells in peripheral nerves. *Nat. Rev. Neurosci.* **6**, 671-682. doi:10.1038/nrn1746

Lara-Gonzalez, P., Westhorpe, F. G. and Taylor, S. S. (2012). The spindle assembly checkpoint. *Curr. Biol.* **22**, R966-R980. doi:10.1016/j.cub.2012.10.006

Lu, M. S. and Johnston, C. A. (2013). Molecular pathways regulating mitotic spindle orientation in animal cells. *Development* **140**, 1843-1856. doi:10.1242/dev.087627

Lyons, D. A., Pogoda, H. M., Voas, M. G., Woods, I. G., Diamond, B., Nix, R., Arana, N., Jacobs, J. and Talbot, W. S. (2005). erbb3 and erbb2 are essential for Schwann cell migration and myelination in zebrafish. *Curr. Biol.* **15**, 513-524. doi:10.1016/j.cub.2005.02.030

Ma, Y., Kanakousaki, K. and Buttitta, L. (2015). How the cell cycle impacts chromatin architecture and influences cell fate. *Front. Genet.* **6**, 19. doi:10.3389/fgene.2015.00019

Michailov, G. V., Sereda, M. W., Brinkmann, B. G., Fischer, T. M., Haug, B., Birchmeier, C., Role, L., Lai, C., Schwab, M. H. and Nave, K. A. (2004). Axonal neuregulin-1 regulates myelin sheath thickness. *Science* **304**, 700-703. doi:10.1126/science.1095862

Mikdache, A., Fontenas, L., Albadri, S., Revenu, C., Loisel-Duwattez, J., Lesport, E., Degerny, C., Del Bene, F. and Tawk, M. (2020). Elmo1 function, linked to Rac1 activity, regulates peripheral neuronal numbers and myelination in zebrafish. *Cell. Mol. Life Sci.* **77**, 161-177. doi:10.1007/s00018-019-03167-5

Mikdache, A., Boueid, M. J., Van Der Spek, L., Lesport, E., Delespierre, B., Loisel-Duwattez, J., Degerny, C. and Tawk, M. (2021). Rgs4 is a regulator of mTOR activity required for motoneuron axon outgrowth and neuronal development in zebrafish. *Sci. Rep.* **11**, 13338. doi:10.1038/s41598-021-92758-z

Mogha, A., Benesh, A. E., Patra, C., Engel, F. B., Schoneberg, T., Liebscher, I. and Monk, K. R. (2013). Gpr126 functions in Schwann cells to control differentiation and myelination via G-protein activation. *J. Neurosci.* **33**, 17976-17985. doi:10.1523/JNEUROSCI.1809-13.2013

Monk, K. R., Feltri, M. L. and Taveggia, C. (2015). New insights on Schwann cell development. *Glia* **63**, 1376-1393. doi:10.1002/glia.22852

Nave, K. A. and Salzer, J. L. (2006). Axonal regulation of myelination by neuregulin 1. *Curr. Opin. Neurobiol.* **16**, 492-500. doi:10.1016/j.conb.2006.08.008

Naveed, M., Kazmi, S. K., Amin, M., Asif, Z., Islam, U., Shahid, K. and Tehreem, S. (2018). Comprehensive review on the molecular genetics of autosomal recessive primary microcephaly (MCPH). *Genet. Res.* **100**, e7. doi:10.1017/S0016672318000046

Nodari, A., Zambroni, D., Quattrini, A., Court, F. A., D'urso, A., Recchia, A., Tybulewicz, V. L., Wrabetz, L. and Feltri, M. L. (2007). Beta1 integrin activates Rac1 in Schwann cells to generate radial lamellae during axonal sorting and myelination. *J. Cell Biol.* **177**, 1063-1075. doi:10.1083/jcb.200610014

Nodari, A., Previtali, S. C., Dati, G., Occhi, S., Court, F. A., Colombelli, C., Zambroni, D., Dina, G., Del Carro, U., Campbell, K. P. et al. (2008). Alpha6beta4 integrin and dystroglycan cooperate to stabilize the myelin sheath. *J. Neurosci.* **28**, 6714-6719. doi:10.1523/JNEUROSCI.0326-08.2008

Novorol, C., Burkhardt, J., Wood, K. J., Iqbal, A., Roque, C., Coutts, N., Almeida, A. D., He, J., Wilkinson, C. J. and Harris, W. A. (2013). Microcephaly models in the developing zebrafish retinal neuroepithelium point to an underlying defect in metaphase progression. *Open Biol.* **3**, 130065. doi:10.1098/rsob.130065

Paavola, K. J., Sidik, H., Zuchero, J. B., Eckart, M. and Talbot, W. S. (2014). Type IV collagen is an activating ligand for the adhesion G protein-coupled receptor GPR126. *Sci. Signal.* **7**, ra76. doi:10.1126/scisignal.2005347

Pereira, J. A., Lebrun-Julien, F. and Suter, U. (2012). Molecular mechanisms regulating myelination in the peripheral nervous system. *Trends Neurosci.* **35**, 123-134. doi:10.1016/j.tins.2011.11.006

Petersen, S. C., Luo, R., Liebscher, I., Giera, S., Jeong, S. J., Mogha, A., Ghidinelli, M., Feltri, M. L., Schöneberg, T., Piao, X. et al. (2015). The adhesion GPCR GPR126 has distinct, domain-dependent functions in Schwann cell development mediated by interaction with laminin-211. *Neuron* **85**, 755-769. doi:10.1016/j.neuron.2014.12.057

Petry, S. (2016). Mechanisms of mitotic spindle assembly. *Annu. Rev. Biochem.* **85**, 659-683. doi:10.1146/annurev-biochem-060815-014528

Pfaff, K. L., Straub, C. T., Chiang, K., Bear, D. M., Zhou, Y. and Zon, L. I. (2007). The zebrafish cassiopeia mutant reveals that SIL is required for mitotic spindle organization. *Mol. Cell. Biol.* **27**, 5887-5897. doi:10.1128/MCB.00175-07

Raphael, A. R. and Talbot, W. S. (2011). Chapter one – new insights into signaling during myelination in zebrafish. *Curr. Top. Dev. Biol.* **97**, 1-19. doi:10.1016/B978-0-12-385975-4.00007-3

Raphael, A. R., Lyons, D. A. and Talbot, W. S. (2011). ErbB signaling has a role in radial sorting independent of Schwann cell number. *Glia* **59**, 1047-1055. doi:10.1002/glia.21175

Sherman, D. L. and Brophy, P. J. (2005). Mechanisms of axon ensheathment and myelin growth. *Nat. Rev. Neurosci.* **6**, 683-690. doi:10.1038/nrn1743

Sztal, T. E., Sonntag, C., Hall, T. E. and Currie, P. D. (2012). Epistatic dissection of laminin-receptor interactions in dystrophic zebrafish muscle. *Hum. Mol. Genet.* **21**, 4718-4731. doi:10.1093/hmg/dds312

Tingaud-Sequeira, A., Raldúa, D., Lavie, J., Mathieu, G., Bordier, M., Knoll-Gellida, A., Rambeau, P., Coupry, I., André, M., Malm, E. et al. (2017). Functional validation of ABHD12 mutations in the neurodegenerative disease PHARC. *Neurobiol. Dis.* **98**, 36-51. doi:10.1016/j.nbd.2016.11.008

Tricaud, N. (2018). Myelinating Schwann cell polarity and mechanically-driven myelin sheath elongation. *Front. Cell Neurosci.* **11**, 414. doi:10.3389/fncel.2017.00414

Woodhoo, A. and Sommer, L. (2008). Development of the Schwann cell lineage: from the neural crest to the myelinated nerve. *Glia* **56**, 1481-1490. doi:10.1002/glia.20723

Yamada, H., Denzer, A. J., Hori, H., Tanaka, T., Anderson, L. V. B., Fujita, S., Fukuta-Ohi, H., Shimizu, T., Rueff, M. A. and Matasumura, J. (1996). Dystroglycan is a dual receptor for Agrin and Laminin-2 in Schwann cell membrane. *J. Biol. Chem.* **271**, 23418-23423. doi:10.1074/jbc.271.38.23418

Yang, D., Bierman, J., Tarumi, Y. S., Zhong, Y. P., Rangwala, R., Proctor, T. M., Miyagoe-Suzuki, Y., Takeda, S., Miner, J. H., Sherman, L. S. et al. (2005). Coordinate control of axon defasciculation and myelination by laminin-2 and −8. *J. Cell Biol.* **168**, 655-666. doi:10.1083/jcb.200411158

Yu, W. M., Feltri, M. L., Wrabetz, L., Strickland, S. and Chen, Z. L. (2005). Schwann cell-specific ablation of Laminin 1 causes apoptosis and prevents proliferation. *J. Neurosci.* **25**, 4463-4472. doi:10.1523/JNEUROSCI.5032-04.2005

Zaqout, S., Morris-Rosendahl, D. and Kaindl, A. M. (2017). Autosomal recessive primary microcephaly (MCPH): an update. *Neuropediatrics* **48**, 135-142. doi:10.1055/s-0037-1601448
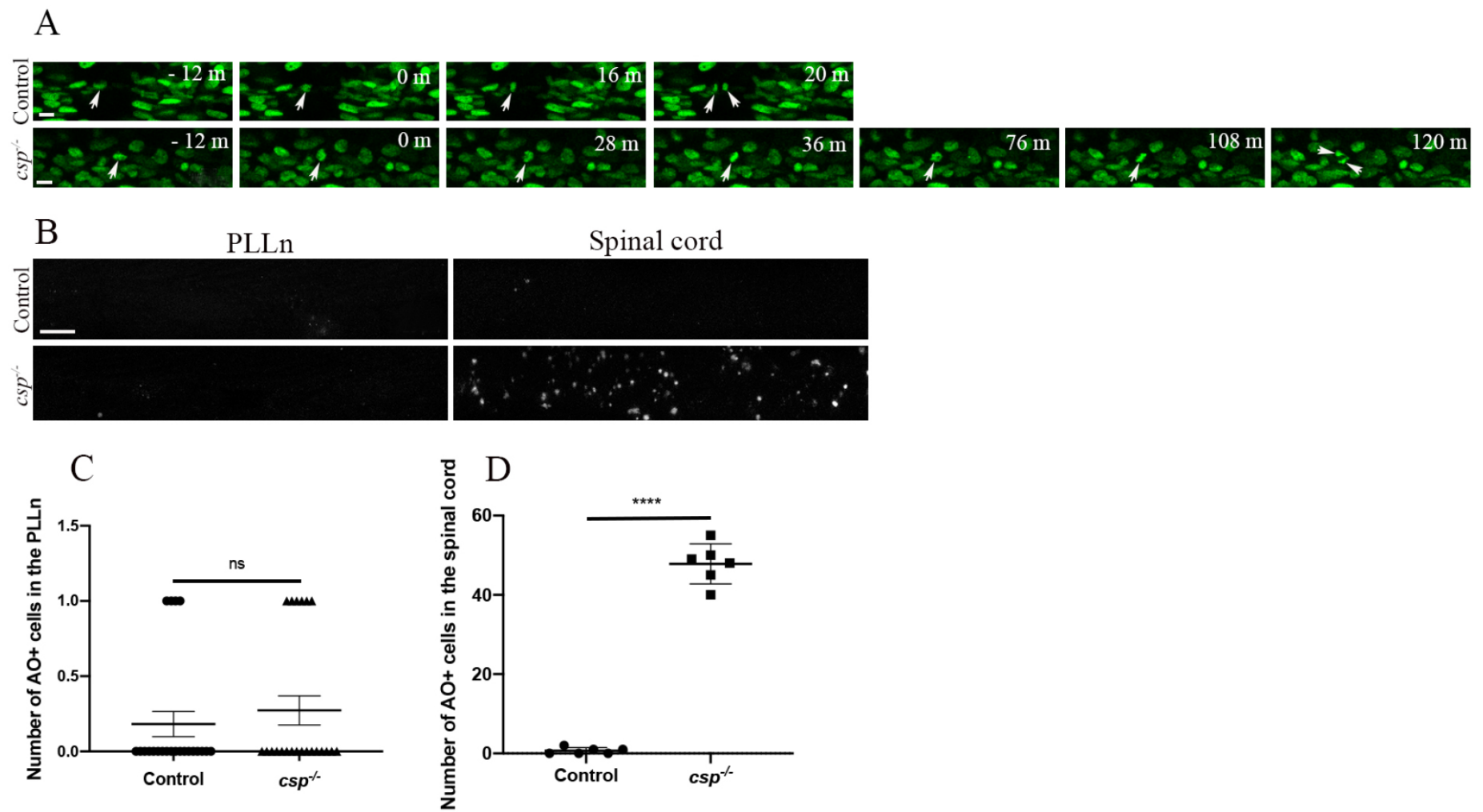
Fig. Sl. SC in *csp*$^{-/-}$ show delays in mitotic progression but exit mitosis with no significant increase in apoptosis

(A) Still images of time-lapse imaging in control (average of 16.67±1.22 min, 6 nuclei, n=3 embryos) and *csp*$^{-/-}$ (average of 98.67±4.55 min, 6 nuclei, n=3 embryos) embryos injected with *h2b:gfp (****, p .5: 0.0001)*. Arrows indicate SC nuclei from the beginning of M phase (time 0) when mitotic rounding takes place until the two nuclei split. Scale bars= 10 μm. m, minutes.

(B) Acridine orange (AO) staining at 50 hpf in control and *csp*$^{-/-}$ embryos within a defined region of the PLLn and spinal cord. Scale bar = 25 μm.

(C) Quantification of the number of AO positive cells in control (average of 0.18±0.08, n=11 embryos) and *csp*$^{-/-}$ (average of 0.27±0.09, n=11 embryos) within a defined region of the PLLn (ns, p=0.72).

(D) Quantification of the number of AO positive cells in control (average of 0.66±0.33, n=6 embryos) and *csp*$^{-/-}$ (average of 47.83±2.05, n=6 embryos) within a defined region of the spinal cord (****, p ≤ 0.0001).
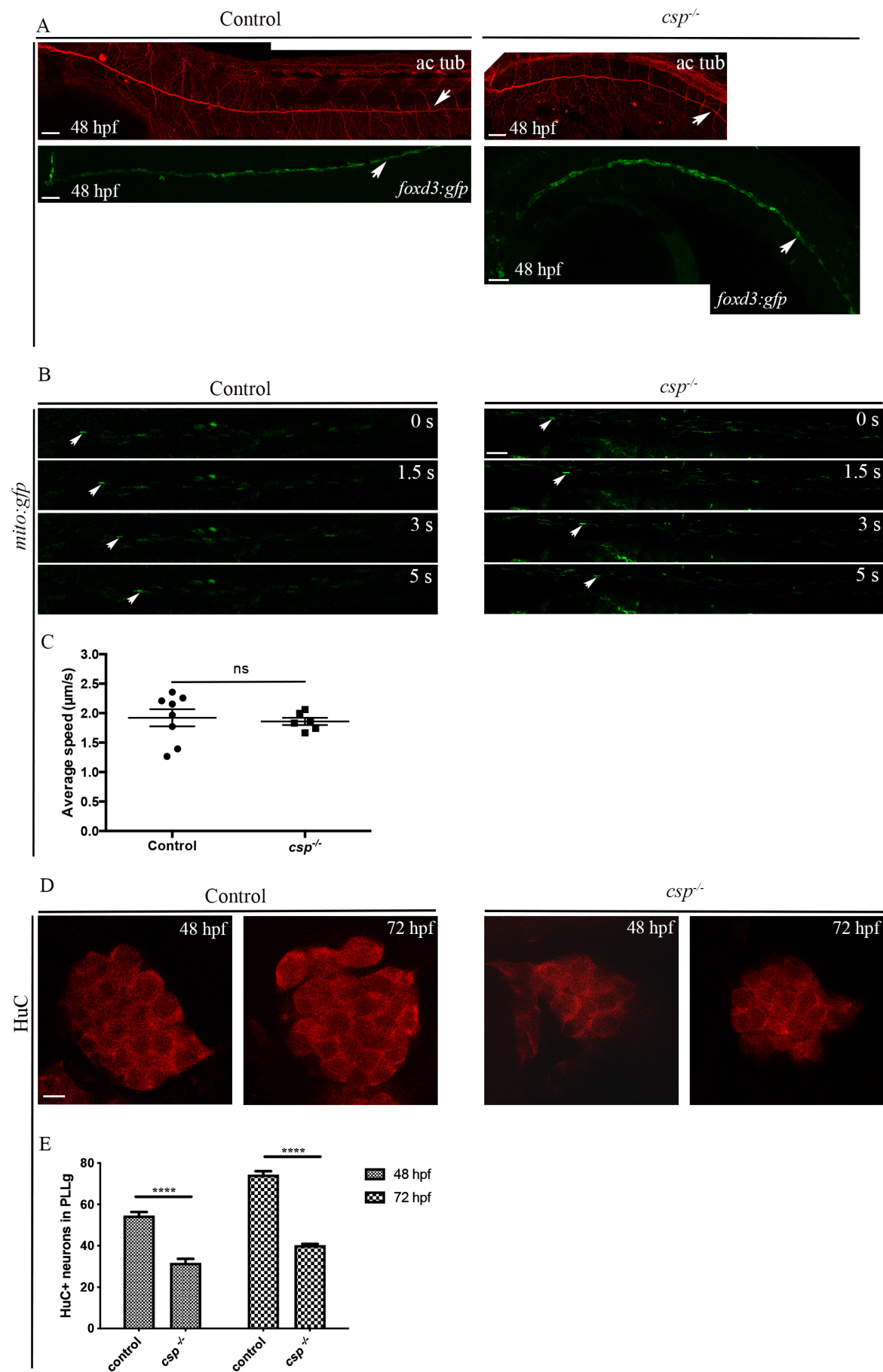
Fig. S2. Sil is not required for axonal growth nor for mitochondrial axonal transport along the PLLn but regulates the number of neurons within the PLLg

(A) Acetylated tubulin expression in a control embryo (n=12) and $csp^{-/-}$·embryo (n=13) at 48 hpf showing the PLLn nerve (arrows). Lateral views of a control (n=16) and $csp^{-/-}$·embryo (n=11) at 48 hpf showing PLLn GFP-expressing SC (arrows). Scale bars = 50 µm.

(B) Still images from time-lapse imaging in control and $csp^{-/-}$ embryos injected with *mito:gfp*. Arrows point to the same mitochondria followed through time in control and $csp^{-/-}$. Scale bar = 5µm.s, seconds.

(C) Quantification of the average speed of mitochondria along the PLLn at 50 hpf in controls (302 mitochondria, n = 8 embryos) and $csp^{-/-}$·embryos (93 mitochondria, n = 6 embryos) (ns, p=0.6976).

(D) HuC immuno-labeling of the PLLg at 48 and 72 hpf in control and $csp^{-/-}$ embryos. Scale bar = µm.

(E) Quantification of the number of neurons in the PLLg at 48 hpf in control (average of 54.58±5.99 neurons, n = 12) and $csp^{-/-}$ (average of 31.71±5.31 neurons, n = 7) embryos and at 72 hpf in control (average of 74.33±5. 88 neurons, n = 12) and $csp^{-/-}$ (40.29± 1.60 neurons n = 7) embryos (****, p.≤ 0.0001 ; ****, p.≤ 0.0001).
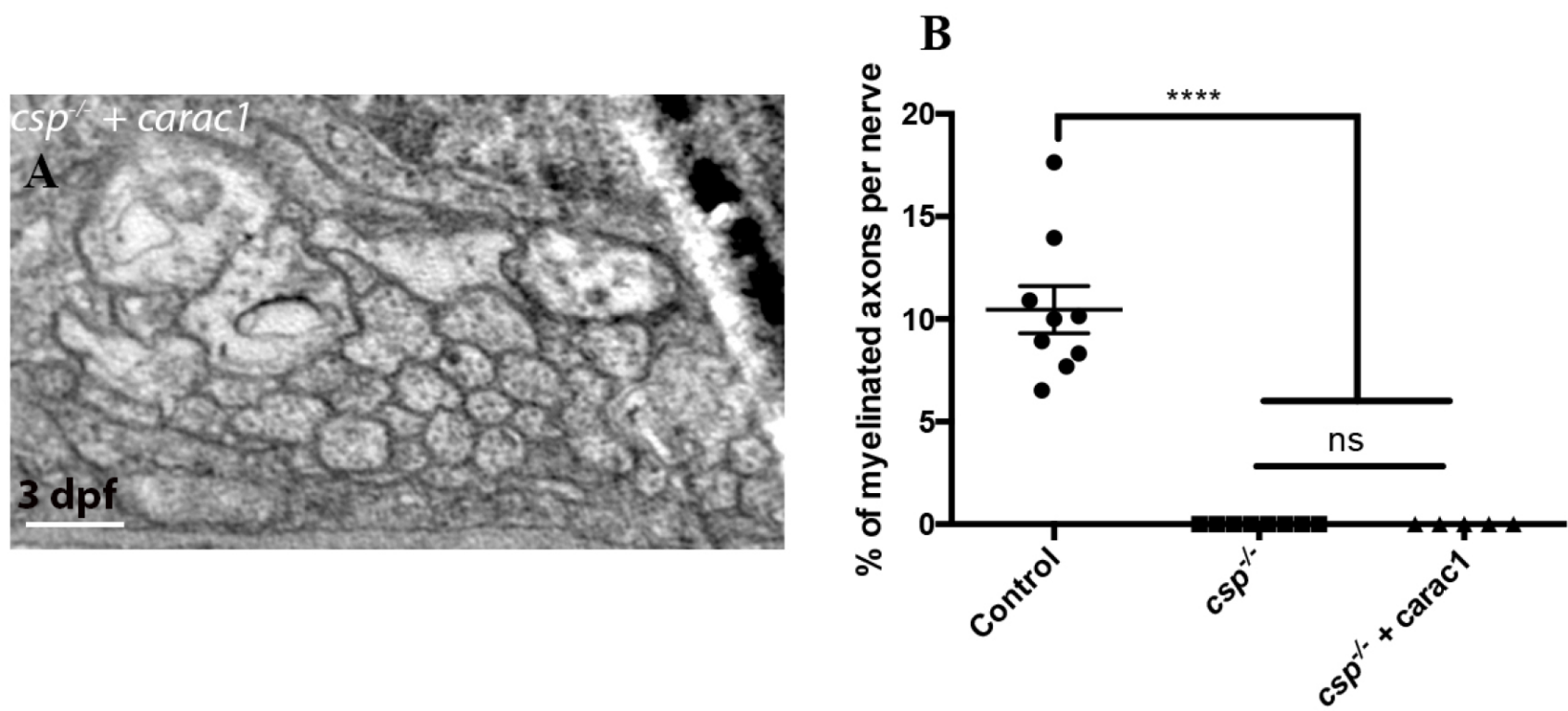
**Fig. S3. Forcing Rael activity does not rescue radial sorting and myelination defects in *csp*^{-/-}**

(A) TEM of a cross section of the PLLn at 3 dpf in *csp*^{-/-} embryo injected with a constitutive active form of Rael *(carael)*. Scale bar 0.5 μm.

(B) Quantification of the percentage of myelinated axons relative to the total number of axons per nerve at 3 dpf in controls (average of 10.5±1.13), *csp*^{-/-} (average ofO)and *csp*^{-/-} injected with *earacl* (average of O) (****, p ≤ 0.0001 , ns, p ≥ 0.999).
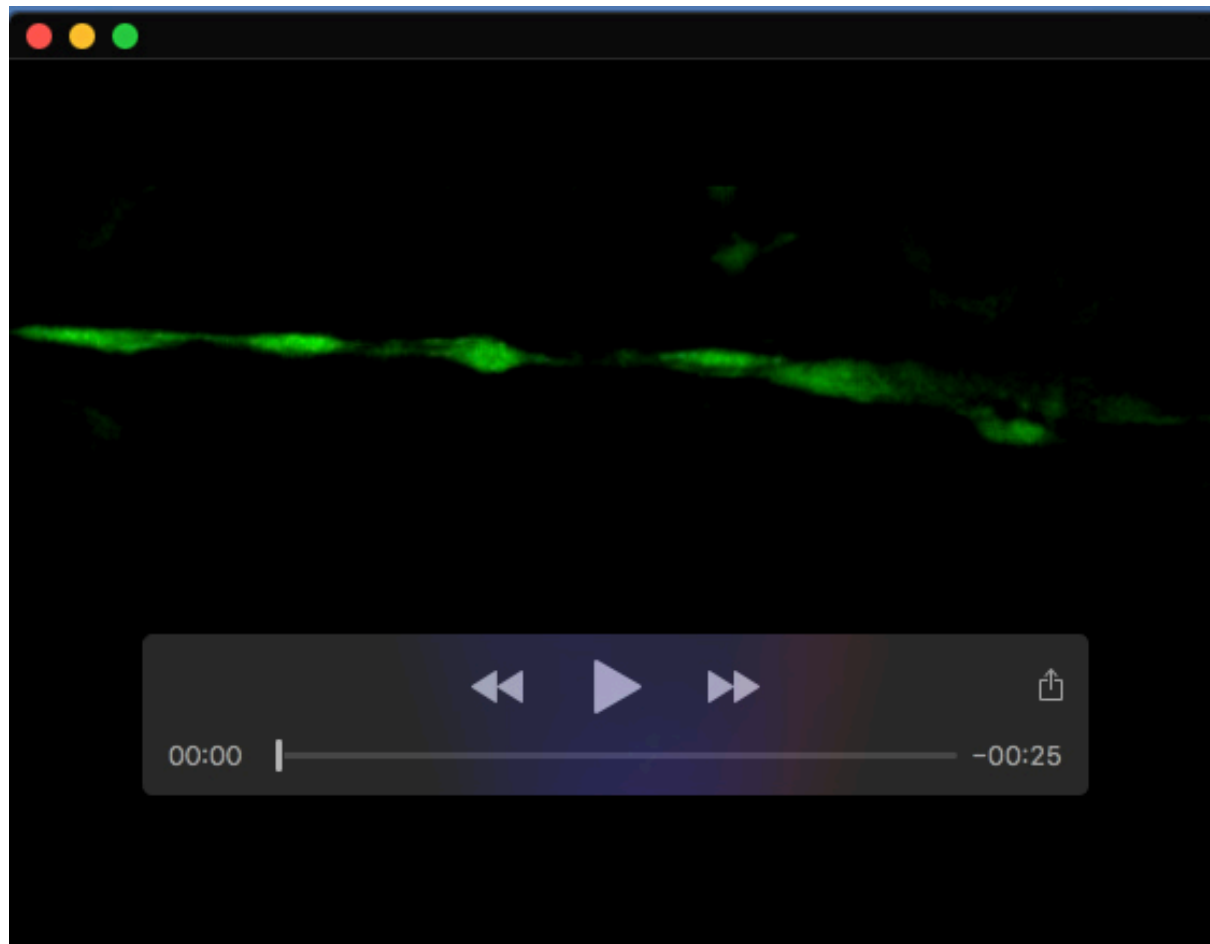
Movie 1. Real-time imaging of SC in *Tg(foxd3:gfp)* embryo at 28 hpf

A 28 hpf embryo expressing GFP in SC; the control embryo was imaged every 4 minutes for several hours by confocal microscopy. Lateral view; anterior to the left and dorsal to the top. This video represents two hours of continuous real-time imaging.
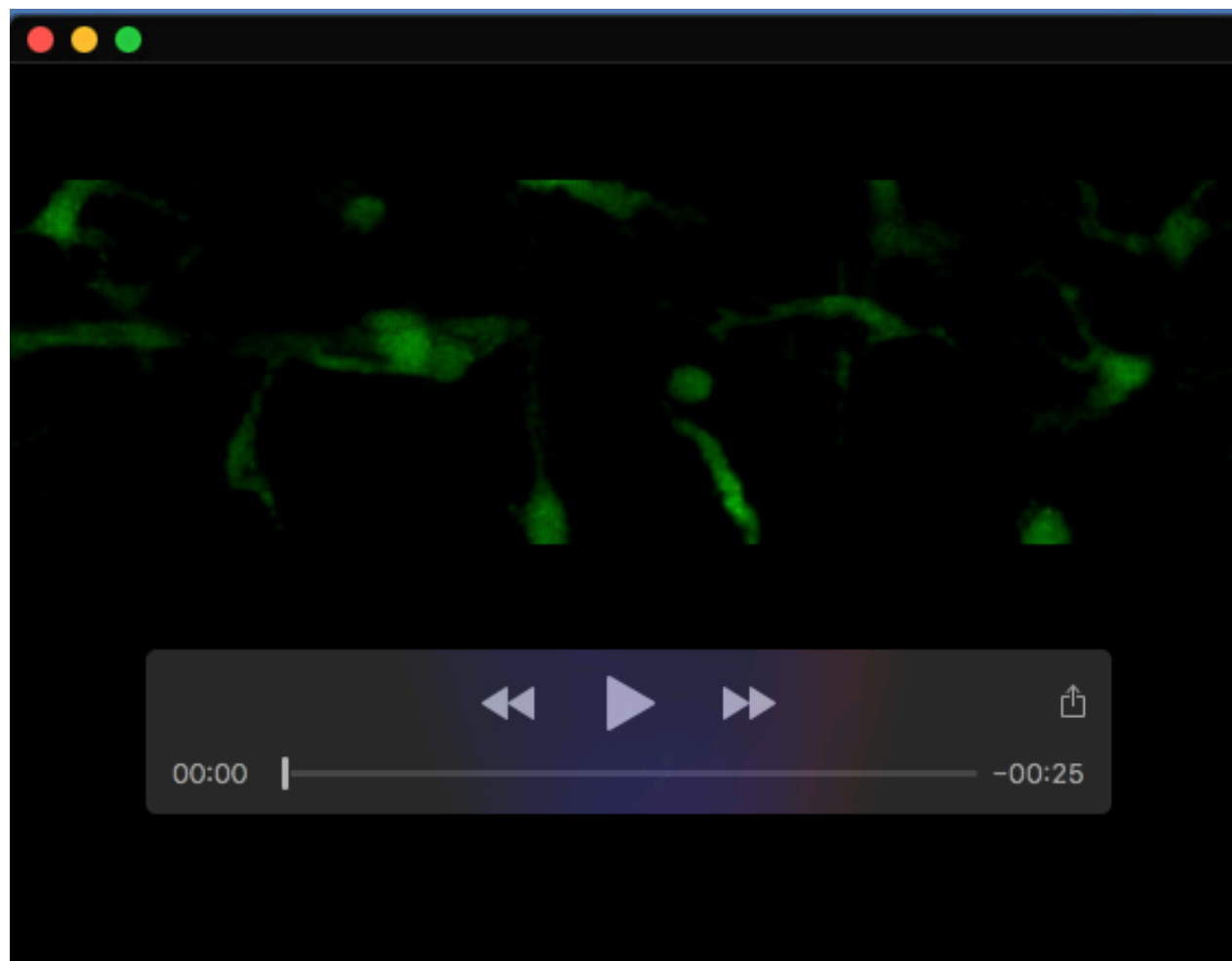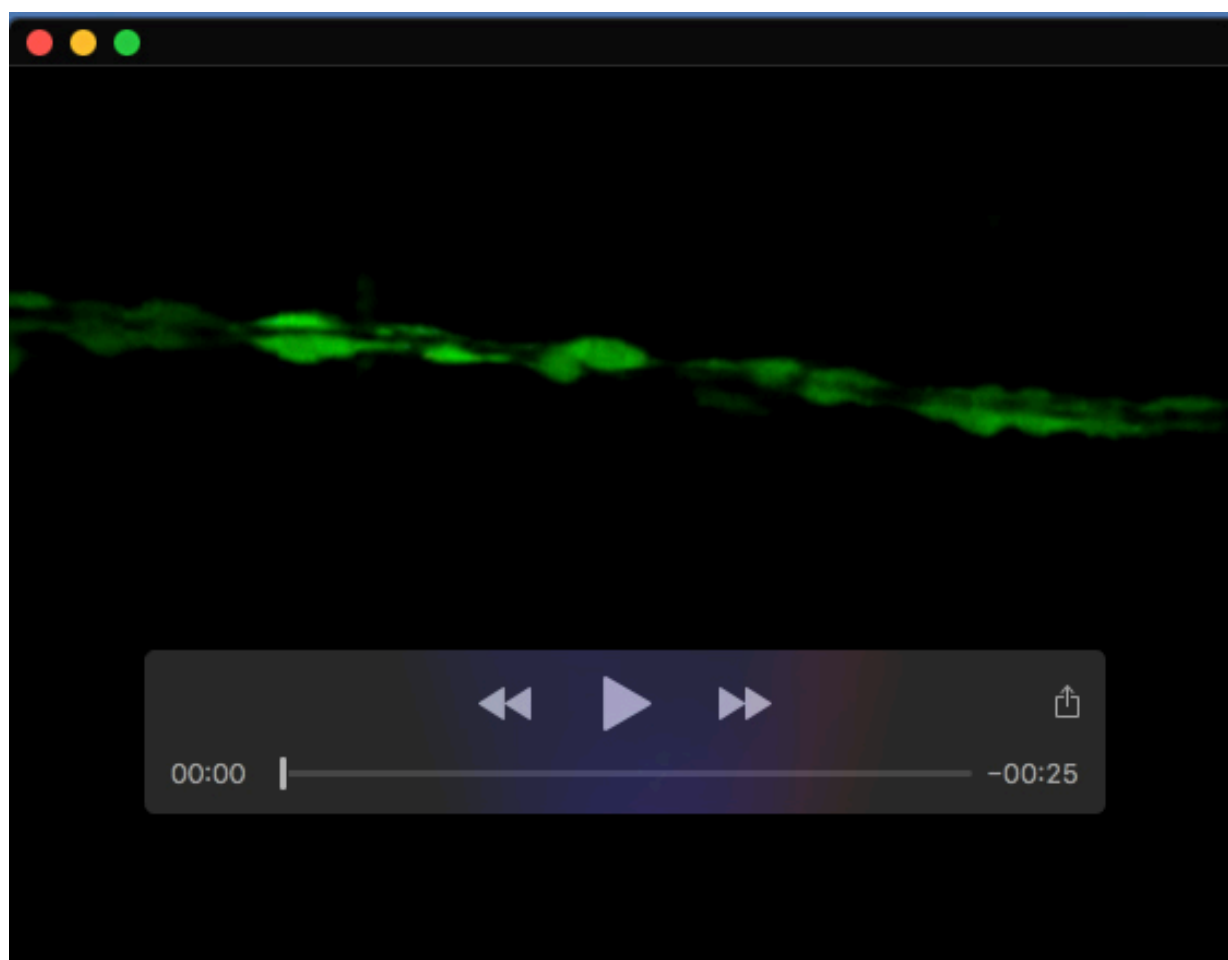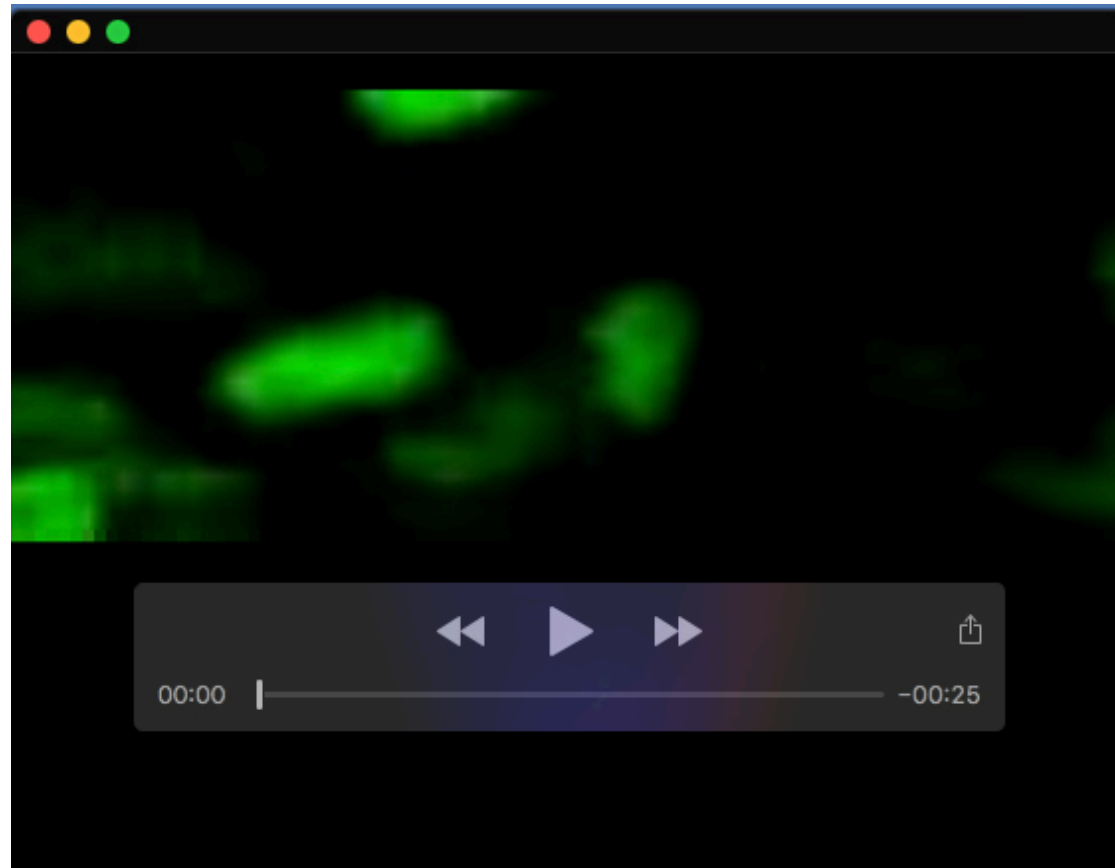

Movie 2. Real-time imaging of SC in *Tg(foxd3:gfp)/ csp-/-* embryo at 28 hpf.

A 28 hpf embryo expressing GFP in SC; the *csp-/-* embryo was imaged every 4 minutes for several hours by confocal microscopy. Lateral view; anterior to the left and dorsal to the top. This video represents four hours of continuous real-time imaging.
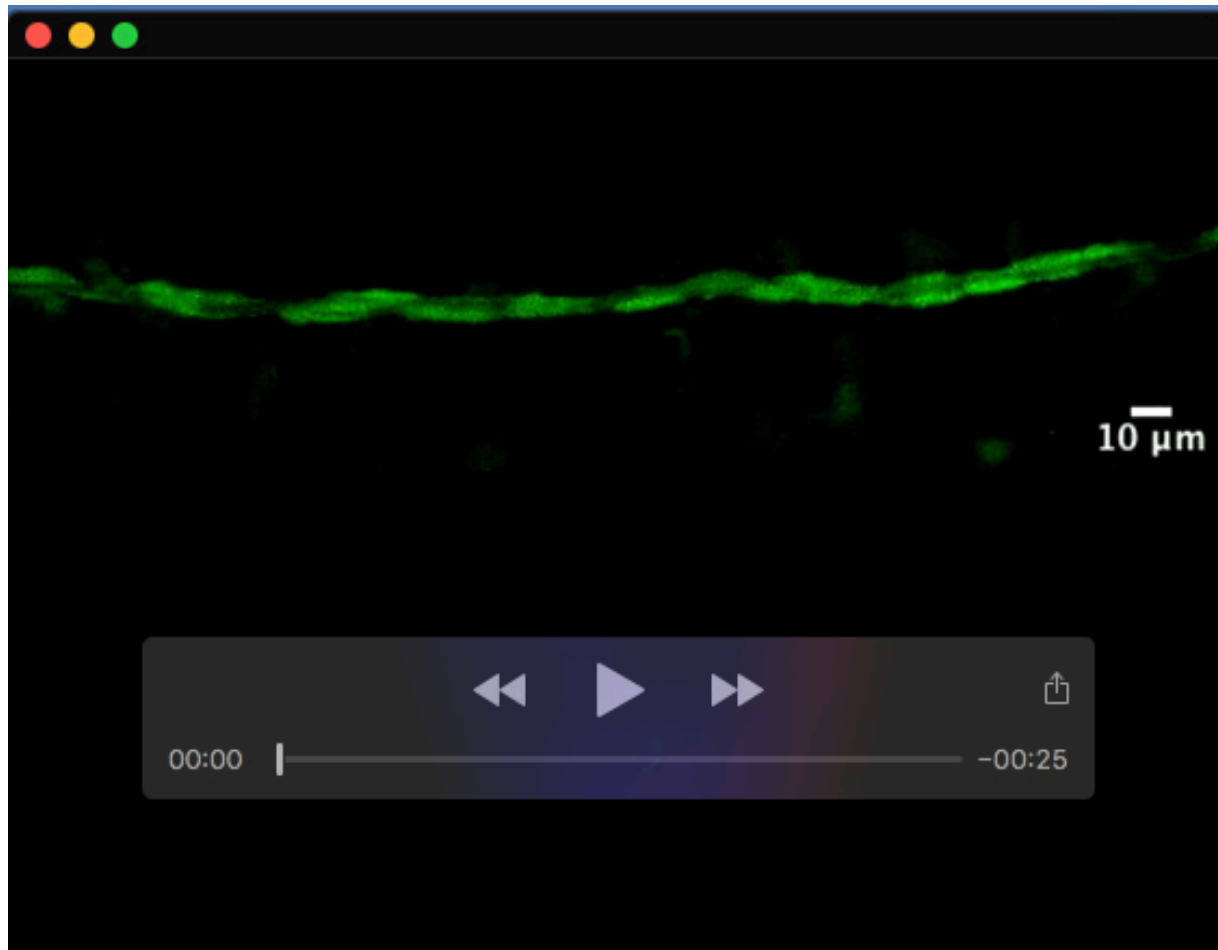
Movie 3. Real-time imaging of SC in *Tg(foxd3:gfp)* embryo at 48 hpf.

A 48 hpf embryo expressing GFP in SC; the control embryo was imaged every 4 minutes for several hours by confocal microscopy. Lateral view; anterior to the left and dorsal to the top. This video represents four and a half hours of continuous real-time imaging.
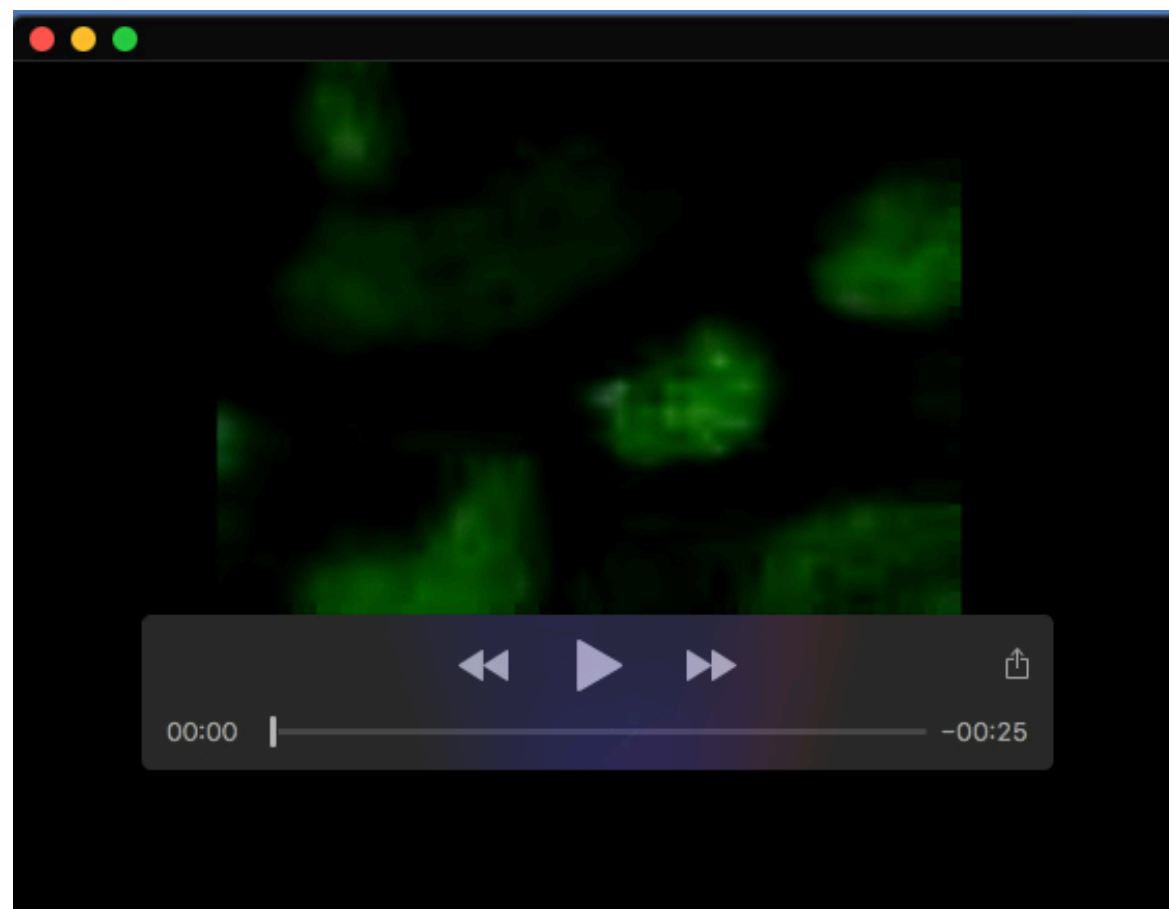

Movie 4. Real-time imaging of SC in *Tg(foxd3:gfp)/ csp⁻/⁻* embryo at 48 hpf.

A 48 hpf embryo expressing GFP in SC; the *csp⁻/⁻* embryo was imaged every 4 minutes for several hours by confocal microscopy. Lateral view; anterior to the left and dorsal to the top. This video represents four and a half hours of continuous real-time imaging.
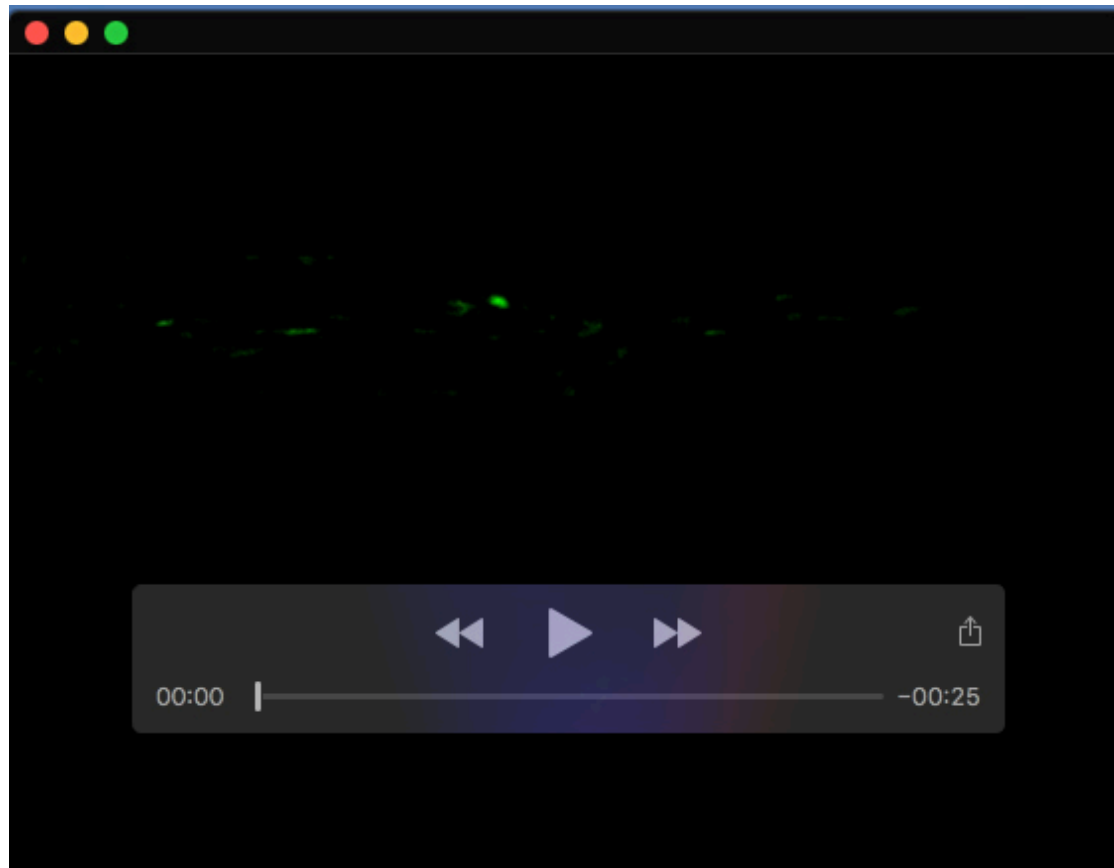
Movie 5. Real-time imaging of SC nuclei in control at 48 hpf.

A 48 hpf control embryo expressing GFP in SC nuclei after *h2b-gfp* mRNA injection; the embryo was imaged every 4 minutes for several hours by confocal microscopy. Lateral view; anterior to the left and dorsal to the top. This video represents 40 minutes of continuous real-time imaging.
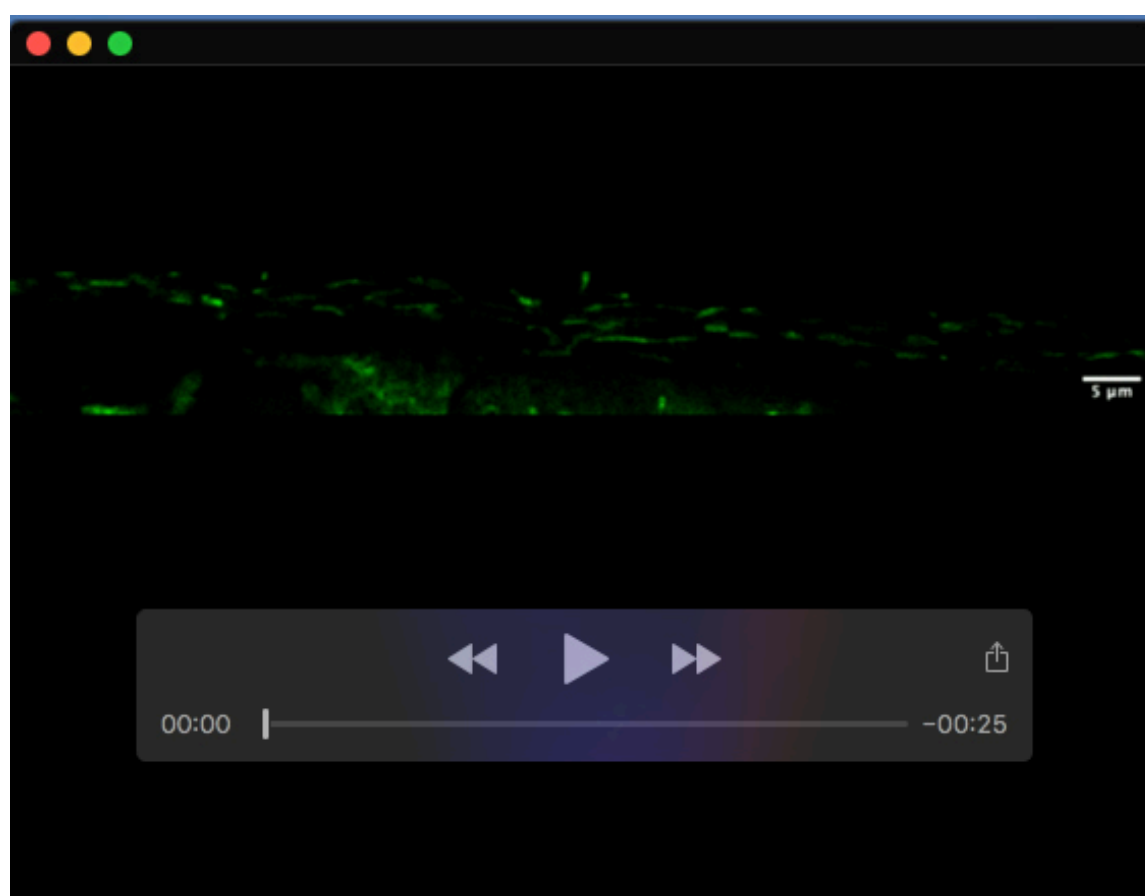

Movie 6. Real-time imaging of SC nuclei in *csp^-/-* at 48 hpf.

A 48 hpf *csp^-/-* embryo expressing GFP in SC nuclei after *h2b-gfp* mRNA injection; the embryo was imaged every 4 minutes for several hours by confocal microscopy. Lateral view; anterior to the left and dorsal to the top. This video represents 100 minutes of continuous real-time imaging.

Movie 7. Real-time imaging of mitochondria in a control PLLn at 48 hpf.

A 48 hpf control embryo expressing GFP in mitochondria after *mito-gfp* mRNA injection; the embryo was imaged every 120 milliseconds for several minutes by confocal microscopy. Lateral view; anterior to the left and dorsal to the top. This video represents 18 seconds of real-time continuous imaging. White arrow highlights an anterograde moving mitochondria while yellow arrow highlights a retrograde moving mitochondria.

Movie 8. Real-time imaging of mitochondria in a *csp*-/- PLLn at 48 hpf.

A 48 hpf *csp*-/- embryo expressing GFP in mitochondria after *mito-gfp* mRNA injection; the embryo was imaged every 120 milliseconds for several minutes by confocal microscopy. Lateral view; anterior to the left and dorsal to the top. This video represents 36 seconds of continuous real-time imaging. White arrow highlights an anterograde moving mitochondria while yellow arrow highlights a retrograde moving mitochondria.